Myosin light chain kinase and Src control membrane dynamics in volume recovery from cell swelling

Elisabeth T. Barfod[a], Ann L. Moore[b], Benjamin G. Van de Graaf[b], and Steven D. Lidofsky[a,b]
Departments of [a]Pharmacology and [b]Medicine, University of Vermont, Burlington, VT 05405

ABSTRACT **The expansion of the plasma membrane, which occurs during osmotic swelling of epithelia, must be retrieved for volume recovery, but the mechanisms are unknown. Here we have identified myosin light chain kinase (MLCK) as a regulator of membrane internalization in response to osmotic swelling in a model liver cell line. On hypotonic exposure, we found that there was time-dependent phosphorylation of the MLCK substrate myosin II regulatory light chain. At the sides of the cell, MLCK and myosin II localized to swelling-induced membrane blebs with actin just before retraction, and MLCK inhibition led to persistent blebbing and attenuated cell volume recovery. At the base of the cell, MLCK also localized to dynamic actin-coated rings and patches upon swelling, which were associated with uptake of the membrane marker FM4-64X, consistent with sites of membrane internalization. Hypotonic exposure evoked increased biochemical association of the cell volume regulator Src with MLCK and with the endocytosis regulators cortactin and dynamin, which colocalized within these structures. Inhibition of either Src or MLCK led to altered patch and ring lifetimes, consistent with the concept that Src and MLCK form a swelling-induced protein complex that regulates volume recovery through membrane turnover and compensatory endocytosis under osmotic stress.**

Monitoring Editor
David G. Drubin
University of California, Berkeley

Received: Jun 16, 2010
Revised: Dec 13, 2010
Accepted: Dec 17, 2010

INTRODUCTION

Rounds of cell swelling and shrinkage accompany a variety of vital biological processes. When these are irreversible, cell death ensues; the ability to recover from perturbations in cell volume is thus a critical aspect of cytoprotection. In the face of osmotic stress induced by stimuli such as solute uptake or hypotonic challenge, there is a rapid increase in cell volume that is followed by volume recovery that occurs despite the continued presence of such stimuli (Schliess *et al.*, 2007; Hoffmann *et al.*, 2009). These changes involve ion channel activation as well as reorganization of the plasma membrane. Although there has been extensive study of volume-sensitive ion channel regulation, considerably less is known about volume-sensitive membrane dynamics.

In a number of cell types, hypotonic challenge evokes exocytosis (Straub *et al.*, 2002; Gatof *et al.*, 2004; Musch *et al.*, 2004), which peaks during the time of cell swelling; this is followed by endocytic membrane retrieval during the time of volume recovery (van der Wijk *et al.*, 2003). Compensatory endocytosis has been observed in response to a variety of stimulated secretory processes (Sokac and Bement, 2006). In hepatocytes, it has been estimated that osmotically stimulated exocytosing vesicles are on the order of 1 μm in diameter (Feranchak *et al.*, 2010). A similar range of vesicle size has been reported in "kiss-and-coat" exocytosis, which has been described in the case of regulated secretion of granule proteins by oocytes and other proteins by specialized epithelia (Bement *et al.*, 2000; Haller *et al.*, 2001; Thorn *et al.*, 2004). In such cases, the compensatory retrieval of vesicles involves actin polymerization and the activity of selected myosin isoforms, including myosin II (Yu and Bement, 2007).

Myosin II modulates endocytic and exocytic events in a broad spectrum of cell functions (Togo and Steinhardt, 2004; Andzelm *et al.*, 2007; Rey *et al.*, 2007; Jiang *et al.*, 2010), as does its regulator myosin light chain kinase (MLCK). For example, MLCK has been

This article was published online ahead of print in MBoC in Press (http://www.molbiolcell.org/cgi/doi/10.1091/mbc.E10-06-0514) on January 5, 2011.

Address correspondence to: Steven Lidofsky (steven.lidofsky@uvm.edu).

Abbreviations used: CTXB, cholera toxin B subunit; GFP, green fluorescent protein; MLC2, myosin II regulatory light chain; mAb, monoclonal antibody; MLCK, myosin light chain kinase; pY, phosphotyrosine; RFP, red fluorescent protein; ROCK, Rho kinase; YFP, yellow fluorescent protein.

shown to control the extent of pore opening and vesicle retrieval in epithelial cells (Bhat and Thorn, 2009). MLCK has also been shown to regulate myosin II–dependent endocytosis of a tight junction protein to control stimulus-dependent epithelial barrier function (Marchiando *et al.*, 2010). Whether MLCK participates in membrane retrieval in cell volume recovery from osmotic swelling is unknown.

Hypotonic challenge and related forms of osmotic cell swelling can evoke the formation of transient dynamic membrane protrusions or blebs, which then resolve during volume recovery (Wilkerson *et al.*, 1986; Worrell *et al.*, 1989; Barfod *et al.*, 2005). We have previously shown that the tyrosine kinase Src, a cell volume regulator (Cohen, 2005), localizes to blebs upon hepatocellular swelling (Barfod *et al.*, 2005). Blebbing has also been observed in other physiological contexts, such as cytokinesis or cell migration (Charras, 2008). Information about Src and its role in physiological blebbing has been limited, but targeting of Src to blebs has been linked to invasiveness of cultured tumor cells (Tournaviti *et al.*, 2007). Src has also been implicated in diverse modes of endocytosis (Shajahan *et al.*, 2004; Kasahara *et al.*, 2007; Sverdlov *et al.*, 2007; Cao *et al.*, 2010), but it is unknown whether Src regulates membrane internalization in response to osmotic stress. We have therefore investigated the roles of MLCK and Src in control of membrane dynamics during volume recovery from cell swelling.

Here we provide evidence that in response to cell swelling, MLCK and Src associate in a complex that regulates a form of compensatory membrane retrieval. This complex localizes with the Src substrates cortactin and dynamin at actin-coated sites of apparent membrane internalization. Our findings further suggest that MLCK and Src play overlapping but distinct roles in the formation and turnover of these sites, which is critical for volume recovery.

RESULTS

Blebs expand during cell swelling with accumulation of actin and myosin II before retraction

Osmotic cell swelling causes dynamic changes in plasma membrane tension, which can create mechanical stresses on the proteins that link the membrane and underlying cortical actin cytoskeleton. When the stresses are sufficiently large, localized disruption of these linkages can lead to membrane blebbing. Indeed, we have previously observed that upon hypotonic swelling, membrane blebs form in some cells (Barfod *et al.*, 2005). In response to mechanical stresses that do not alter cell volume, blebs are retracted through the action of actin-based motor proteins, including myosin II (Charras *et al.*, 2008). To determine whether myosin II localized to blebs during hypotonic exposure, we performed live imaging of HTC hepatoma cells transfected with an red fluorescent protein (RFP) fusion of the MLC2 regulatory light chain of myosin II (also known as RLC) to label myosin II, and with green fluorescent protein (GFP)–farnesyl to label membranes. We found that the membranous regions of blebs that formed upon hypotonic exposure were initially devoid of myosin II. Shortly before retraction, RFP-MLC2 accumulated at the periphery of some blebs (Figure 1A, Supplemental Figure S1). To see whether actin was also involved in bleb retraction, the experiment was repeated with cells that were transfected with membrane-targeted RFP-farnesyl (here pseudocolored in green for comparison to Figure 1B) and with GFP-actin (here pseudocolored in red). As with observations concerning MLC2 localization upon cell swelling, we found that actin did not accumulate at the bleb periphery until bleb retraction began (Figure 1B, Supplemental Figure S2). These data support a role for myosin II and actin in bleb retraction during osmotic stress.

In physiological processes that do not involve changes in cell volume, blebbing does not appear to involve insertion of new membrane (Charras, 2008). By contrast, osmotic cell swelling (e.g., produced by hypotonic challenge) is associated with a marked increase in membrane turnover (van der Wijk *et al.*, 2003). The time period of volume-sensitive exocytosis in liver cells (Feranchak *et al.*, 2010) overlaps with the time period of blebbing that we have observed under similar conditions of hypotonic exposure (Barfod *et al.*, 2005), suggesting that bleb expansion during osmotic stress could include contributions of membrane from within the cell. Consistent with this concept, we have observed in cells that were exposed to the membrane probe FM4-64X (which fluoresces only when intercalated into membranes) a focal transient decrease in FM4-64X fluorescence at the periphery of blebs upon swelling (Supplemental Figure S3A). This raised the possibility that mechanisms of regulation of bleb dynamics during osmotic challenge may be distinct from those in other forms of mechanical stress.

MLCK phosphorylates MLC2 in response to cell swelling and regulates bleb retraction and volume recovery

The activity of myosin II is regulated primarily by serine/threonine phosphorylation of MLC2 (Vicente-Manzanares *et al.*, 2009). If myosin II were participating in regulation of membrane dynamics during osmotic stress, it would be predicted that there would be time-dependent changes in MLC2 phosphorylation in response to hypotonic challenge. To test this, we used phosphospecific MLC2 antibodies for immunoblot analysis of lysates of cells exposed to isotonic or hypotonic media for different durations. On hypotonic exposure, there was a time-dependent increase in the abundance of mono (S19) and diphosphorylated (T18S19) forms of MLC2 (Figure 1C, Supplemental Figure S3C).

Among the diverse proteins that modulate MLC2 phosphorylation, MLCK and Rho kinase (ROCK) appear to play complementary roles in the establishment and maintenance of cortical actin tension, with ROCK localized predominantly to the cell center and MLCK to the cell periphery (Totsukawa *et al.*, 2004). To determine whether either kinase played a role in the response to cell swelling, we compared the MLC2 phosphorylation response to hypotonic exposure in the presence versus absence of MLCK inhibitor ML-7 and the ROCK inhibitor Y27632, respectively. We found that ML-7, but not Y27632, inhibited swelling-induced MLC2 phosphorylation (Supplemental Figure S3D), implicating a role for MLCK in this process.

Given that myosin II localized to the plasma membrane in association with bleb retraction, we tested whether MLCK was recruited in a similar way. We examined this in cells expressing GFP-MLCK and RFP-actin. We found that upon hypotonic exposure, GFP-MLCK, like myosin II, was translocated to bleb peripheries, where it colocalized with RFP-actin (Figure 1D, Supplemental Figure S4). To ensure that the apparent MLCK recruitment to blebs was not due simply to MLCK binding to actin as a result of actin overexpression, we performed parallel experiments in which GFP-MLCK was expressed with the membrane marker RFP-farnesyl and observed a similar localization to bleb peripheries (marked by the farnesyl signal) in response to cell swelling (Supplemental Figure S3E). In conjunction with the observations above, these findings support the hypothesis that swelling-induced translocation of MLCK activates myosin II at the plasma membrane to facilitate bleb retraction during hypotonic stress.

To test this, we performed live imaging of cells under conditions of MLCK inhibition. We found that upon hypotonic exposure in the presence of ML-7, membrane blebbing was persistent (Figure 1, E and F; Supplemental Video 1). In particular, long after volume recovery typically occurred in control cells (~30 min), membrane blebs could still be observed in the presence of ML-7. Inhibition of MLCK

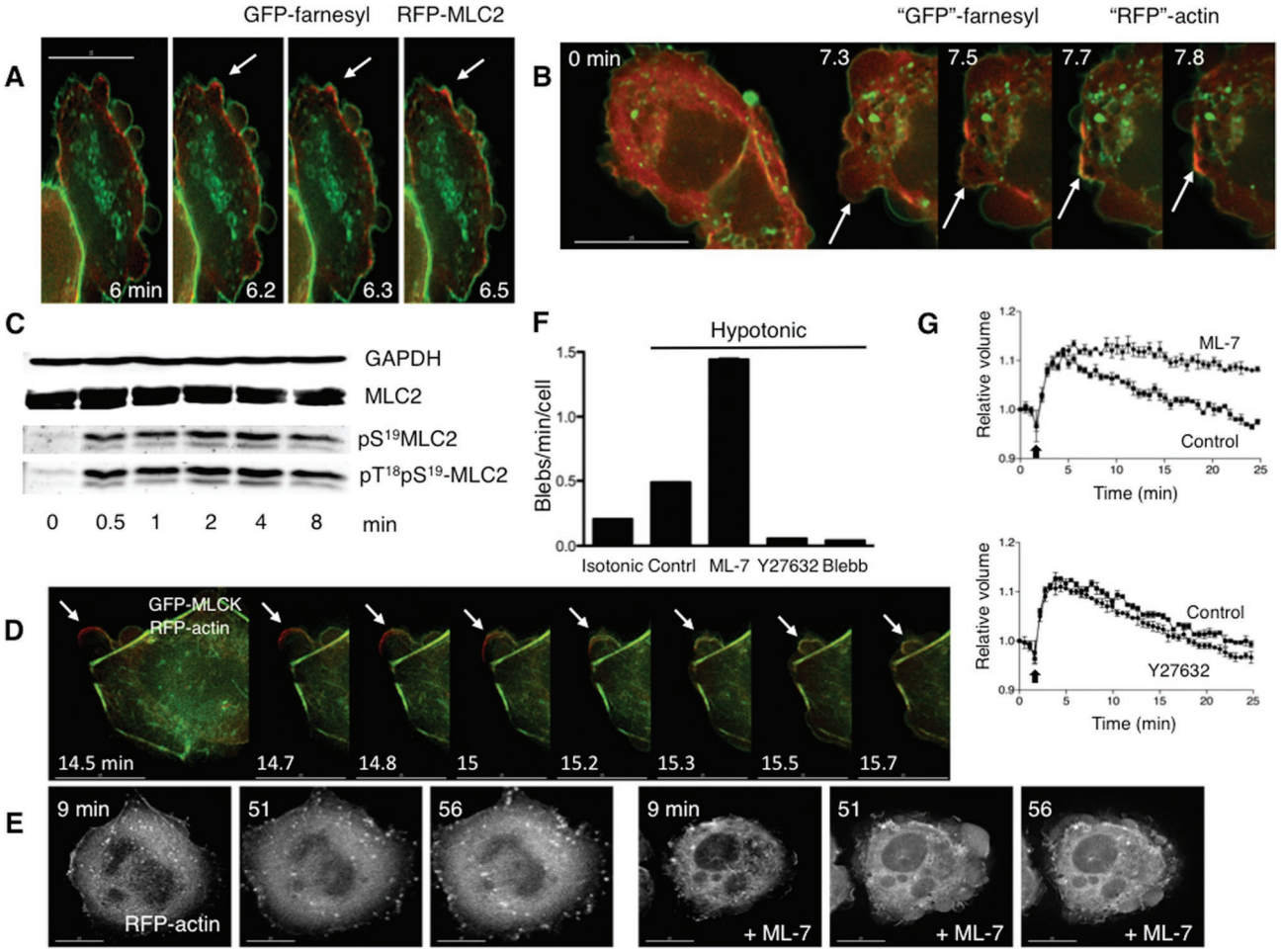

FIGURE 1: Roles for MLCK in bleb dynamics and cell volume recovery. (A) Sequential stills from a live imaging study of swollen cells transfected with farnesyl-GFP (green), to mark membranes, and RFP-MLC2 (red), to mark myosin II. Arrows mark a bleb that retracts. (B) Sequential stills from a live imaging study of cells transfected with farnesyl-RFP (pseudocolored green) and GFP-actin (pseudocolored red) and then swollen. Arrows mark a bleb that retracts. The scale bar in all images is 15 μm, and the time (in min) indicates duration of hypotonic exposure. (C) Cell swelling induces increases in phosphorylation of the regulatory light chain of myosin II (MLC2). Representative immunoblot for MLC2 and its phosphorylated forms in response to hypotonic exposure. Whole cell lysates were prepared from cells swollen for the times denoted. (D) Stills from live images in cells transfected with RFP-actin (red) and GFP-MLCK (green) show that MLCK is recruited to blebs before their retraction. An arrow marks a spot where a bleb retracts. (E) Stills at early and late time points in a live imaging study of swollen cells transfected with RFP-actin show that inhibition of MLCK with ML-7 (10 μM) leads to persistent blebbing far beyond the typical time of volume recovery (see graphs in G). (F) Effects of inhibitors of MLCK (ML-7), ROCK (Y27632), and myosin II (blebbistatin) on swelling-induced blebbing. Depicted are numbers of blebs per min per cell under isotonic conditions (far left) and with hypotonic exposure in the absence (Contrl) or presence of ML-7 (10 μM), Y27632 (10 μM), or blebbistatin (Blebb, 30 μM). (G) Effects of ML-7 (top, 10 μM) and Y27632 (bottom, 10 μM) on cell volume compared with no inhibitor present (Control), after hypotonic exposure. An arrow marks the switch to hypotonic exposure. Data were compiled from at least three experiments for each condition.

also occasionally led to the extreme phenotype called circus movement, in which blebs move tangentially around the cell (Charras *et al.*, 2008) (see Supplemental Video 2). In contrast, the ROCK inhibitor Y27632 suppressed bleb formation upon hypotonic exposure (Figure 1F), and the membrane expanded uniformly (compare Supplemental Videos 1 and 3). Global suppression of myosin II–dependent tension with blebbistatin also suppressed hypotonically induced bleb formation (Figure 1F, Supplemental Video 5). Intriguingly, in cells that were blebbing under isotonic conditions, the subsequent addition of blebbistatin at the time of hypotonic exposure did not suppress further bleb enlargement, and the actin cortex could appear sheared (Supplemental Figure S3F), consistent with a function for myosin II in maintaining the integrity of the actin cortex during cell swelling. Similar cortical breaks were seen in cells treated with ML-7 (Supplemental Figure S3G), raising the possibility that MLCK is responsible for maintaining actin cortical integrity during osmotic stress.

In nonosmotic blebbing, Src has been reported to regulate bleb formation through ROCK (Tournaviti *et al.*, 2007). However, whereas ROCK inhibition did not affect MLC2 phosphorylation upon swelling, Src inhibition with PP2, like inhibition of MLCK, attenuated swelling-induced MLC2 phosphorylation (Supplemental Figure S3D).

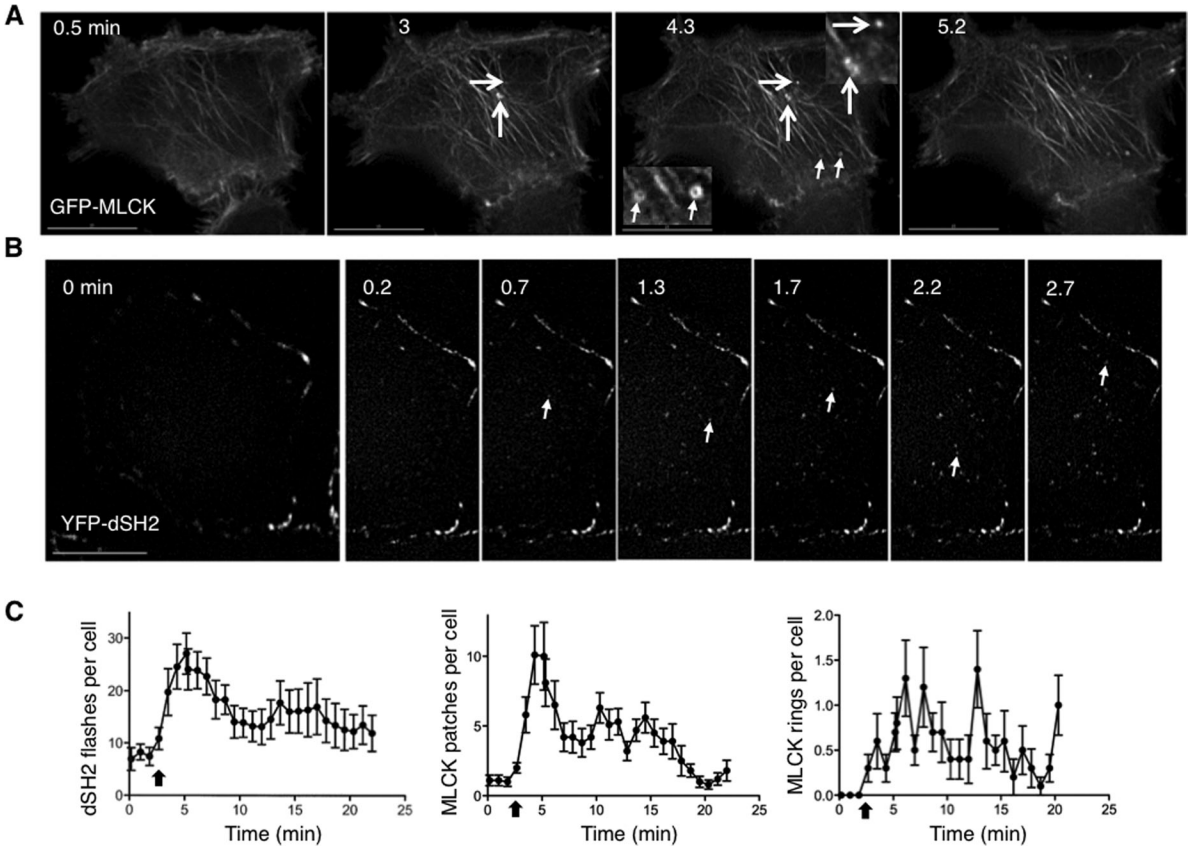

FIGURE 2: Swelling induces localization of MLCK to foci at the base of the cell, where focal transient tyrosine phosphorylation events are detected. (A) Selected stills from a swollen cell expressing GFP-MLCK show the appearance and disappearance of rings and patches. Representative patches are marked with larger arrows; representative rings are marked with smaller arrows. Insets at higher magnification are marked with the same arrows. (B) Stills taken at the base of a cell overexpressing YFP-dSH2 before and after hypotonic exposure. Arrows mark new dSH2 flashes, sites of tyrosine phosphorylation, at each time point. Time (in min) indicates duration of hypotonic exposure. (C) Graphs of the number of YFP-dSH2 flashes per cell (left) and the number of GFP-MLCK patches (middle) and rings (right) per cell as a function of time. The kinetics of the dSH2 flashes and MLCK patches follow a similar time course. Scale bars are 15 μm.

This suggests that Src may mediate MLCK kinase activity during cell volume recovery, consistent with our finding that activated Src is recruited to bleb membranes before retraction (Barfod *et al.*, 2005). Thus, with MLCK inhibition during cell swelling, ROCK-dependent myosin II tension is unopposed and pulls the weakened actin cortex against the hydrostatic force pushing out, so that localized cortical separation occurs and blebs form. When blebbistatin relaxes both the ROCK and MLCK-mediated myosin II tensions, cells swell but do not develop blebs. Collectively, these observations support the concept that Src-activated MLCK (through myosin II), but not ROCK, regulates swelling-induced bleb retraction.

Intriguingly, MLCK has been suggested to regulate volume recovery in response to osmotic cell swelling (Nilius *et al.*, 2000; Shen *et al.*, 2002), but this has not been examined directly. We therefore tested whether inhibition of this kinase influenced cell volume responses to hypotonic challenge. Consistent with a role for MLCK in the process, we found that ML-7 (but not the ROCK inhibitor Y27632) attenuated cell volume recovery (Figure 1G). Given that cell swelling under these conditions is accompanied by exocytosis (Feranchak *et al.*, 2010), these findings collectively support the hypothesis that volume recovery is facilitated by MLCK-mediated membrane retrieval, although it is possible that in bleb retraction, MLCK might act by harnessing membrane contraction with retrograde flow (Giannone *et al.*, 2004).

MLCK also appears as motile patches and rings at the base of the cell in a time frame concomitant with transient phosphotyrosine signals

MLCK-regulated bleb retraction appears to be one of the responses to cell swelling. However, it cannot fully account for the dependence of cell volume recovery on MLCK activity per se because not all swollen cells bleb (Supplemental Video 4). We therefore hypothesized that MLCK also regulates retrieval of membranes outside of blebs during osmotic stress and looked for localization of MLCK to other dynamic membrane structures. On swelling of GFP-MLCK–expressing cells, we observed two other motile MLCK-positive structures at the base: rings and patches that were ~0.5 μm in diameter (Figure 2A, Supplemental Video 7). Although patches could be occasionally and transiently visualized under isotonic conditions, they appeared more prominently after hypotonic exposure (Figure 2C).

Patches of actin mark sites of endocytosis in yeast (Mulholland *et al.*, 1994), and they have been found at sites of classic clathrin-coated pits in mammalian cells (Merrifield *et al.*, 2005; Yarar *et al.*, 2005). Larger clathrin-coated endocytic structures, similar in size to those of the swelling-induced MLCK patches, have also been reported (Saffarian *et al.*, 2009). Intriguingly, actin rings, of the same order of magnitude as the MLCK rings, have been observed

under special conditions that apparently stabilize the association between cytoskeletal proteins and the clathrin-dependent endocytic machinery (Engqvist-Goldstein *et al.*, 2004). Thus swelling induced MLCK structures at the base of the cell resemble previously described actin-based structures that are associated with membrane internalization.

Given the roles for Src in diverse modes of endocytosis, we hypothesized that Src facilitated the recruitment of MLCK to volume-sensitive patches and rings. This was based upon our previous observations that activated Src (like MLCK reported above) localized to bleb edges in response to cell swelling (Barfod *et al.*, 2005) as well as work by others that the long form of MLCK is a substrate for Src-mediated tyrosine phosphorylation (Birukov *et al.*, 2001). To test whether Src was also activated at the cell base upon cell swelling, we transfected cells with a phosphotyrosine (pY)–binding fluorescent protein fusion made from tandem duplications of the c-Src SH2 domain (YFP-dSH2). Such a fusion can detect Src activators and activated Src (Kirchner *et al.*, 2003; Robles *et al.*, 2005). In response to hypotonic exposure, short-lived puncta of dSH2 signal, which we have called flashes, were seen at the base of the cell (Figure 2B, Supplemental Video 8). Intriguingly, the kinetics of the frequency of flashes elicited by hypotonic exposure resembled the kinetics of cell swelling and volume recovery under parallel conditions (compare left panel of Figure 2C with Figure 1G). To determine whether these flashes correlated with the appearance of MLCK rings and patches at the base of the cell, we counted such structures in GFP-MLCK–expressing cells in response to swelling. Indeed, the kinetics of MLCK patch appearance (Figure 2C, middle panel) were similar to those of flashes (time after hypotonic exposure to peak number of patches, 2.2 ± 0.5 min, vs. time to peak number of flashes, 2.4 ± 0.3 min). These findings suggested that patch formation and pY signaling at the cell base occurred in the same time frame. By contrast, the ring response (Figure 2C, right panel) was not as informative, either because of the small number of events or because ring appearance was more stochastic. Because the kinetics of the Src flashes and appearance of MLCK patches follow the time frame reported for hepatocellular volume-sensitive exocytosis (Feranchak *et al.*, 2010), this provided further support for the possibility that the MLCK patches represented sites of membrane internalization.

Src, actin, and cortactin are localized to swelling-induced MLCK patches

To determine whether Src was the tyrosine kinase responsible for the dSH2 flashes and whether actin was associated with the MLCK structures, we immunostained fixed cells expressing GFP-MLCK and RFP-actin with an antibody specific for activated (pY) Src. On hypotonic exposure, pY-Src and actin were found to be associated with MLCK patches at the cell base (Figure 3A, Supplemental Figure S6).

To pursue this further, we sought the presence in such patches of regulators of endocytosis that might associate with MLCK and Src. We proposed the involvement of the Src substrate cortactin, which regulates actin polymerization (Dudek *et al.*, 2002; Ammer and Weed, 2008), is required for different modes of endocytosis (Cao *et al.*, 2003; Sauvonnet *et al.*, 2005), and can form a complex with the long form of MLCK and Src (Garcia *et al.*, 1999). We therefore reasoned that if MLCK patches represented sites of active membrane retrieval upon swelling, then cortactin would be present in such patches in its tyrosine-phosphorylated form. To test this, we immunostained cells expressing GFP-MLCK and RFP-actin with an antibody specific for pY-cortactin. On hypotonic exposure, pY-cortactin was found to be associated with GFP-MLCK/RFP-actin patches at the cell base (Figure 3A, Supplemental Figure S6). These findings support the hypothesis that upon cell swelling, cortactin and MLCK form a complex with Src in actin patches and that this process involves Src-induced tyrosine phosphorylation. We therefore performed biochemical studies to examine this question further. Following hypotonic exposure, there was a time-dependent increase in the abundance of the long form of MLCK and of pY-cortactin in Src immunoprecipitates (Figure 3B), particularly in membrane fractions (Figure 9A). Moreover, there was a significant correlation between the intensities of pY-Src and MLCK signal in Src immunoprecipitates (Figure 3C; Spearman $r = 0.8678$, $p < 0.0001$). These findings provide further support for a role of Src function in formation of a volume-sensitive complex with cortactin and MLCK and, in conjunction with observations above, raise the possibility that these proteins regulate MLCK/actin patch dynamics.

To examine the temporal association of actin, cortactin, and MLCK in swelling-induced patches, we performed live imaging of cells transfected with GFP-MLCK and RFP-actin or RFP-cortactin during hypotonic challenge. Under these conditions, the dynamics of actin recruitment to patches paralleled that of MLCK (Figure 4A, Supplemental Figure S7, Supplemental Video 9). The association between MLCK and cortactin in patches was different (Figure 4B, Supplemental Figure S8, Supplemental Video 10). Detection of cortactin appeared to precede bulk MLCK signal within patches, and cortactin signal remained constant, while MLCK signal rose and fell as it did with actin. This is reminiscent of the dynamic association between regulators of receptor-mediated endocytosis at sites of membrane internalization (Merrifield *et al.*, 2005).

MLCK rings and patches are likely to be sites of membrane retrieval

Given the possibility that MLCK localized to sites of membrane retrieval following swelling, we asked whether swelling-induced rings and patches at the cell base were associated with membrane structures and internalized membrane markers. We therefore performed live imaging of cells expressing GFP-MLCK and RFP-farnesyl, subjected them to hypotonic challenge, and monitored structures at the base as they formed and disappeared (Figure 5A). We found that MLCK rings could transiently be associated with farnesyl-labeled membrane, either colocalizing with farnesyl rings or encircling a lumen of membrane signal (Figure 5, B and C; Supplemental Figure S9). By contrast, detection of specific farnesyl signal in MLCK patches was not apparent, perhaps because of low signal (Supplemental Figure S10A).

To test whether patches could be labeled by a more sensitive membrane marker, we exposed GFP-MLCK–expressing cells first to isotonic and then to hypotonic medium in the continuous presence of the exogenous membrane dye FM4-64X. On hypotonic exposure, membrane dye signal appeared in association with MLCK structures at the base of cells, including patches (Supplemental Figure S11B, Supplemental Video 11). To ensure that this was not a property of overexpressed MLCK, we also swelled GFP-actin–expressing cells in the presence of FM4-64X. On swelling, membrane signal immediately appeared at structures (including rings and patches) that recruited additional actin in a dynamic manner (Supplemental Figure S11A, Supplemental Video 12). These findings suggest that patches, like rings, are sites of membrane internalization. Intriguingly, under conditions of MLCK inhibition, the membrane signal associated with actin in a more stable manner (Supplemental Figure S11C, Supplemental Video 13), which raises the possibility that the kinase activity of MLCK regulates the dynamics of these structures.

To better determine the fine structure of the rings, we performed experiments with GFP-MLCK–transfected cells, FM4-64X, and

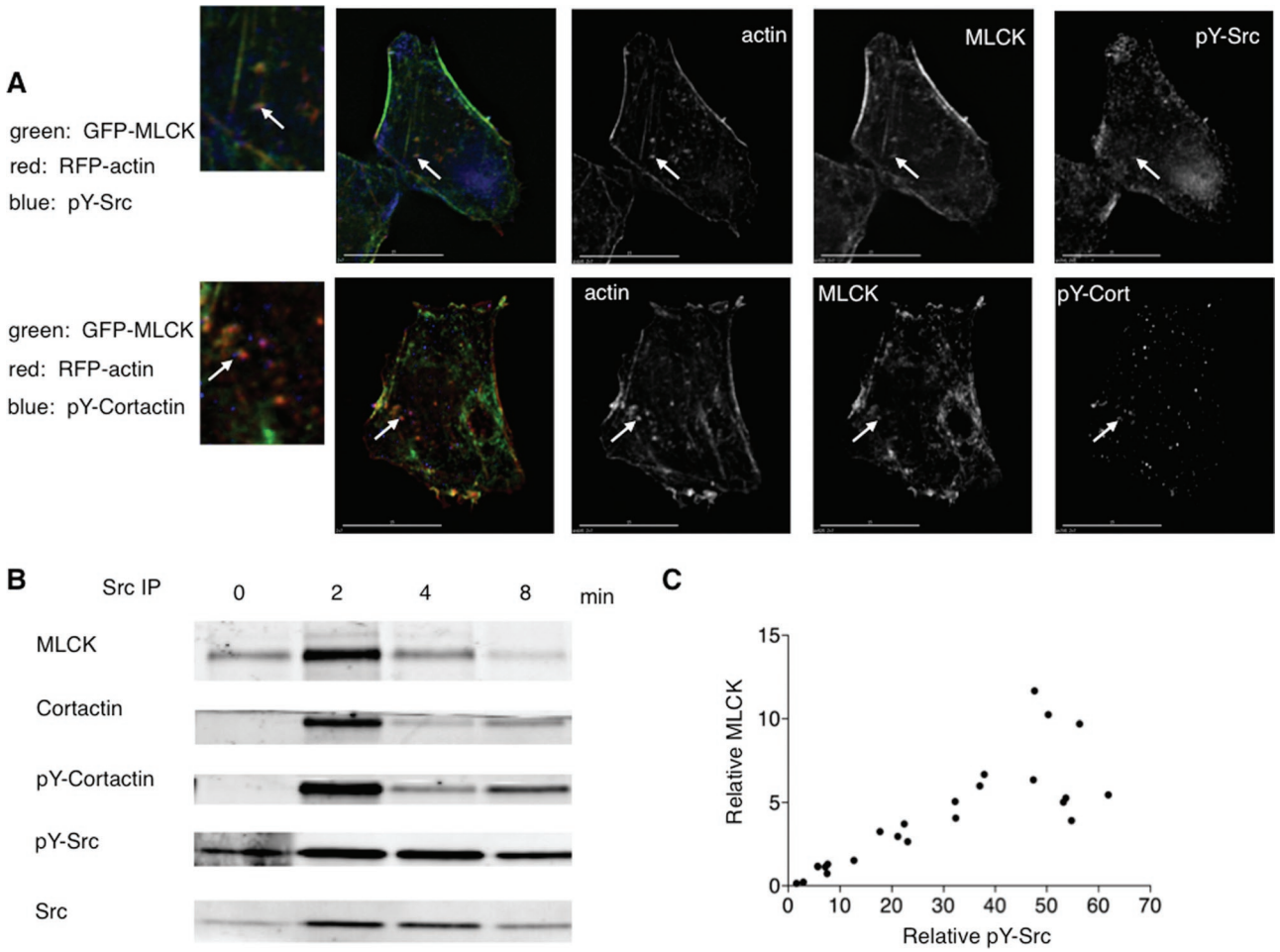

FIGURE 3: Activated pY-Src and pY-cortactin are found associated with actin/MLCK patches, and immunoprecipitation analysis is consistent with a Src/cortactin/MLCK complex formed on cell swelling. (A) Immunostaining of cells fixed 1 min after hypotonic exposure shows that MLCK colocalizes with pY-Src and pY-cortactin in patches at the base. One patch in each cell is marked with an arrow below it. A magnification of the area of interest is marked with the arrow to the left. (B) MLCK association with activated Src is time dependent after cell swelling. Whole cell lysates (1 mg protein) were prepared from cells that underwent hypotonic exposure for the times indicated (time = 0, initial isotonic conditions), and Src immunoprecipitation was performed. A representative immunoblot of the immunoprecipitates is shown. (C) MLCK and pY-Src signals for each time point (including isotonic controls) were divided by the corresponding fold increase in Src (relative to signal at time = 0), in analogy to methods previously described (Barfod *et al.*, 2005). Correlation analysis of six independent experiments shows that MLCK is significantly associated (Spearman $r = 0.8678$, $p < 0.0001$) with pY-Src in Src immunoprecipitates from swollen cells.

fluorescently labeled dextran (10 kDa), a fluid phase marker. In fixed cells that had been swollen, dextran was found within the lumen of a ring of MLCK that also was associated with FM4-64X (Supplemental Figure S10B). In swollen cells transfected with GFP-MLCK and RFP-actin, dextran was found associated within rings containing both MLCK and actin (Supplemental Figure S10C). Three-dimensional reconstruction of this structure indicated that the dextran was entirely encircled by MLCK and actin, consistent with its being taken up from the media and suggesting that rings could be structures that formed during an endocytic event. In rare events, we found that over time, some of the ring structures appeared to become patch structures (Figure 5D, Supplemental Figure S12, Supplemental Video 14). Thus, if rings represent endocytic structures, the detectable internalized farnesyl membrane would imply that rings are intermediates in a macroscale mode of membrane retrieval, and likewise patches (with undetectable farnesyl membrane signal) could represent intermediates in a microscale mode of membrane retrieval (Kumari *et al.*, 2010). It is therefore possible that MLCK is involved in distinct modes of membrane internalization during osmotic stress.

If swelling-induced membrane retrieval at rings or patches proceeds by a mechanism analogous to that of compensatory endocytosis, one expectation is the formation of actin coats at theses sites (Sokac *et al.*, 2003) and coat compression by myosin II (Yu and Bement, 2007). To test whether MLCK kinase function regulates actin association with patches and rings, we performed live imaging of cells transfected with GFP-MLCK and RFP-actin, which were swollen in the presence of ML-7. Despite kinase inhibition, actin still associated with MLCK patches and rings (Figure 6, A and B). Similarly, swelling-induced MLCK rings were observable in cells transfected with mutant, kinase-inactive GFP-MLCK (Supplemental Figure S13E, Supplemental Video 21). To exclude the possibility that these results were influenced by actin binding to overexpressed MLCK, we performed analogous studies in cells expressing GFP-actin alone, which were fixed following hypotonic exposure in the presence of ML-7

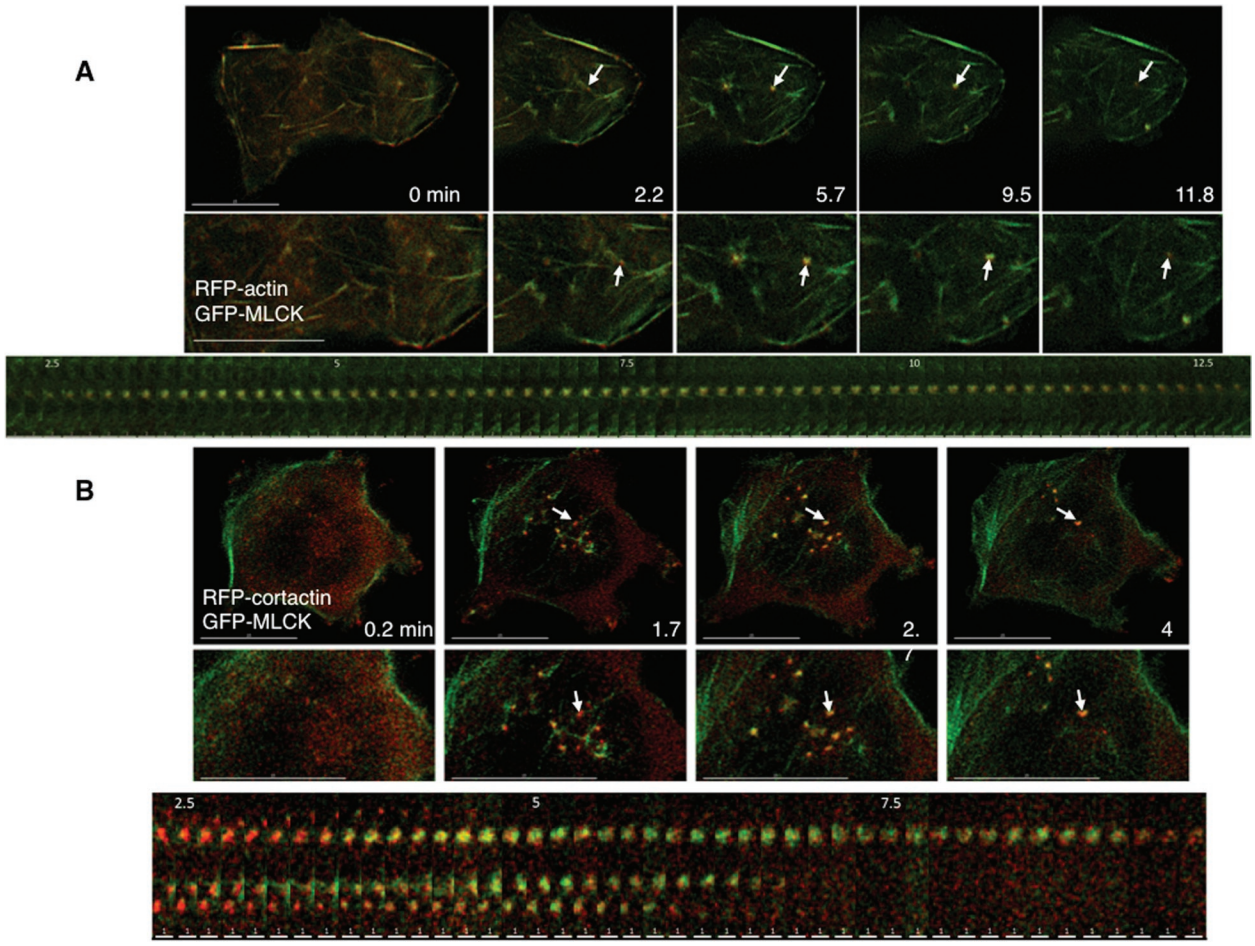

FIGURE 4: Actin and cortactin transiently localize with MLCK at the base of the cell in response to swelling. (A) Stills from live imaging of cells transfected with GFP-MLCK and RFP-actin are depicted at different times (in min) after hypotonic exposure and show simultaneous appearance and disappearance of MLCK (green) and actin (red) to patches at the base of the cell. A patch that is transiently induced by cell swelling is marked with an arrow. A kymograph of the patch indicated in the magnified insets is shown below. (B) Stills from live images of cells transfected with GFP-MLCK (green) and RFP-cortactin (red) at different times (in min) after hypotonic treatment. The midsection of each cell base is magnified below. An arrow indicates simultaneous GFP-MLCK and RFP-cortactin accumulation in patches in response to cell swelling. A kymograph including the patch indicated in the magnified insets is shown below; the top patch is the one marked with an arrow above. Scale bars are 15 μm for the top panels of (A) and (B). The scale bars in the kymograph in (A) are 2 μm and in the kymograph in (B) are 1 μm.

and FM4-64X. Under these conditions, partial and complete GFP-actin rings could be seen at the base of the cell, with morphologies similar to those labeled with MLCK (Figure 6C). Intriguingly, rings of FM4-64X were also observed (Figure 6C), but they did not always overlap with actin. This suggests that membrane rings are platforms for actin polymerization and that the actin polymerization step is independent of the kinase activity of MLCK.

MLCK and Src activity control MLCK patch and ring dynamics

If MLCK/actin patches and rings function as volume-sensitive sites of membrane retrieval, they would be expected to turn over once the membrane has been internalized. Because Src phosphorylation has been implicated in regulation of remodeling of actin-rich structures by cortactin (Head *et al.*, 2003), and because Src-mediated phosphorylation increases the stability of a Src/cortactin/MLCK complex (Dudek *et al.*, 2002), we reasoned that Src kinase activity might influence MLCK recruitment to patches and rings, and Src inhibition would alter their formation or lifetime. To test this, we performed live imaging of GFP-MLCK–expressing cells undergoing hypotonic challenge under conditions of Src inhibition. In the presence of the Src inhibitor PP2, swelling-induced MLCK signal in patches was transient, and stable patches at the base of the cell did not appear to form (Supplemental Video 15). Intriguingly, some PP2-treated cells exhibited MLCK rings at the base of the cell, which increased in number with cell swelling (Supplemental Video 16). These findings support the hypothesis that Src activity regulates swelling-induced MLCK structure dynamics (and by inference compensatory membrane retrieval), in part, by stabilizing MLCK recruitment to patches and/or facilitating ring maturation.

If MLCK plays a role in volume-sensitive MLCK/actin patch dynamics, then manipulating MLCK activity might also influence the morphology and/or lifetime of these structures. To test this, we performed live imaging of GFP-MLCK–expressing cells in the presence or absence of MLCK inhibition. We found that upon hypotonic exposure, ML-7 led to a significant increase in patch diameter

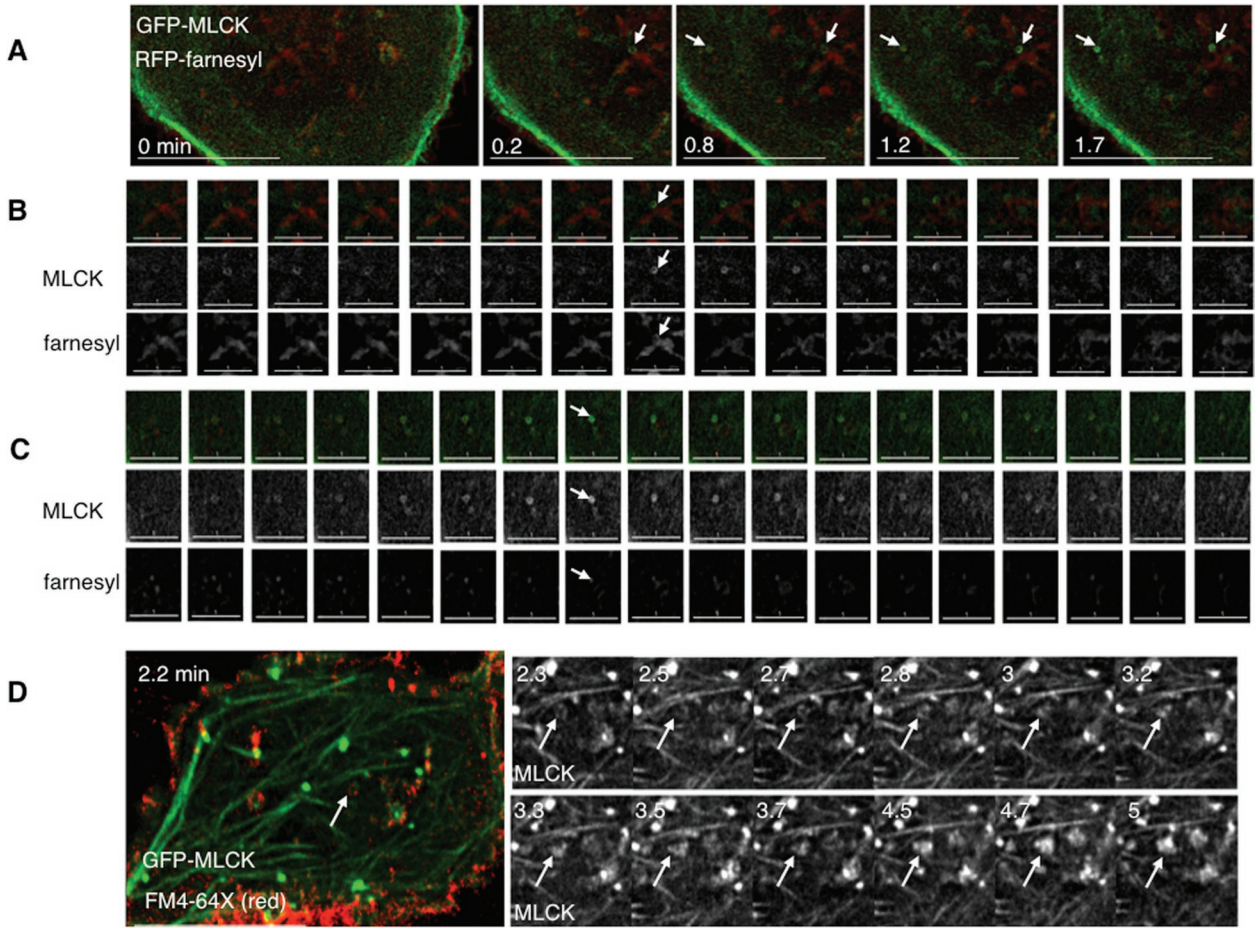

FIGURE 5: GFP-MLCK rings appear to be associated with discrete membrane structures at the base of the cell. (A) Stills taken of cells expressing GFP-MLCK (green) and RFP-farnesyl (red) for different times (in min) after hypotonic treatment. Different angled arrows mark different MLCK rings displayed in the following two panels. Scale bars are 15 μm. (B) Sequential stills of the ring marked by an arrow in the upper right corner of panel A from just before to 2.5 min after hypotonic treatment. The top row shows GFP-MLCK (green) and RFP-farnesyl (red). The middle row shows signal from MLCK, and the bottom row shows signal from farnesyl. The arrow indicates a time (1.2 min after hypotonic exposure) when both MLCK and some of the membrane marker appear as rings. Scale bars are 5 μm. (C) Sequential stills of the ring marked by an arrow in the upper left corner of panel A from 0.7 min to 3.5 min after hypotonic treatment. The top row shows GFP-MLCK (green) and RFP-farnesyl (red). The middle row shows MLCK signal, and the bottom row shows farnesyl signal. The arrow indicates a time (1.8 min) when the lumen of the MLCK ring is filled with membrane marker. Scale bars are 5 μm. (D) Stills from live imaging of cells transfected with GFP-MLCK (green) exposed to exogenous FM4-64X (red) for 2 min during hypotonic treatment and then washed out for the remaining recovery. An arrow marks an area where membrane dye has been internalized, such that GFP-MLCK signal colocalizes with an apparent FM4-64X ring. The adjacent panels depict magnified images of the MLCK signal for subsequent times. Over time, the MLCK ring appears to become a patch. The scale bar is 15 μm.

(0.52 ± 0.02 vs. 0.75 ± 0.04 μm with ML-7, $p = 0.0001$) and a significant increase in patch lifetime (1.7 ± 0.3 vs. 3.5 ± 0.5 min with ML-7, $p = 0.001$) (Supplemental Videos 17 and 18).

To further quantify the effects of the Src and MLCK inhibitors on the dynamics of the structures formed, we counted rings and patches in GFP-MLCK–expressing cells that underwent hypotonic exposure in the absence versus presence of inhibitors (Figure 6, D and E; Supplemental Figure S13). MLCK inhibition partially but significantly reduced the maximum number of patches formed upon swelling (maximum number of patches per cell at peak time: 12.6 ± 2.1 vs. 7.9 ± 0.9 with ML-7, $p = 0.0274$), and Src inhibition significantly attenuated swelling-induced patch formation (maximum number of patches per cell at peak time 12.6 ± 2.1 vs. 4.1 ± 0.6 with PP2, $p = 0.0011$).

ML-7 had more complex effects on ring dynamics. There were no apparent differences in MLCK ring formation between control and ML-7–treated cells under these conditions (Figure 6D, maximum number of rings per cell at peak time 2.3 ± 0.4 vs. 1.9 ± 0.4 with ML-7). In parallel studies of cells expressing RFP-farnesyl, ML-7 increased (relative to the absence of inhibitor) the number of swelling-induced farnesyl membrane rings (Supplemental Figure S13). Intriguingly, in GFP-MLCK– and RFP-farnesyl–coexpressing cells that were treated with ML-7, although the number of MLCK rings did not increase (compared with the absence of inhibitor), the proportion of MLCK rings associated with farnesyl membrane was increased (Supplemental Figure S13). Moreover, in cells expressing GFP-actin, ML-7 led to a similar proportion of actin-associated FM4-64X rings (Supplemental Figure S13). The apparent accumulation with ML-7 of

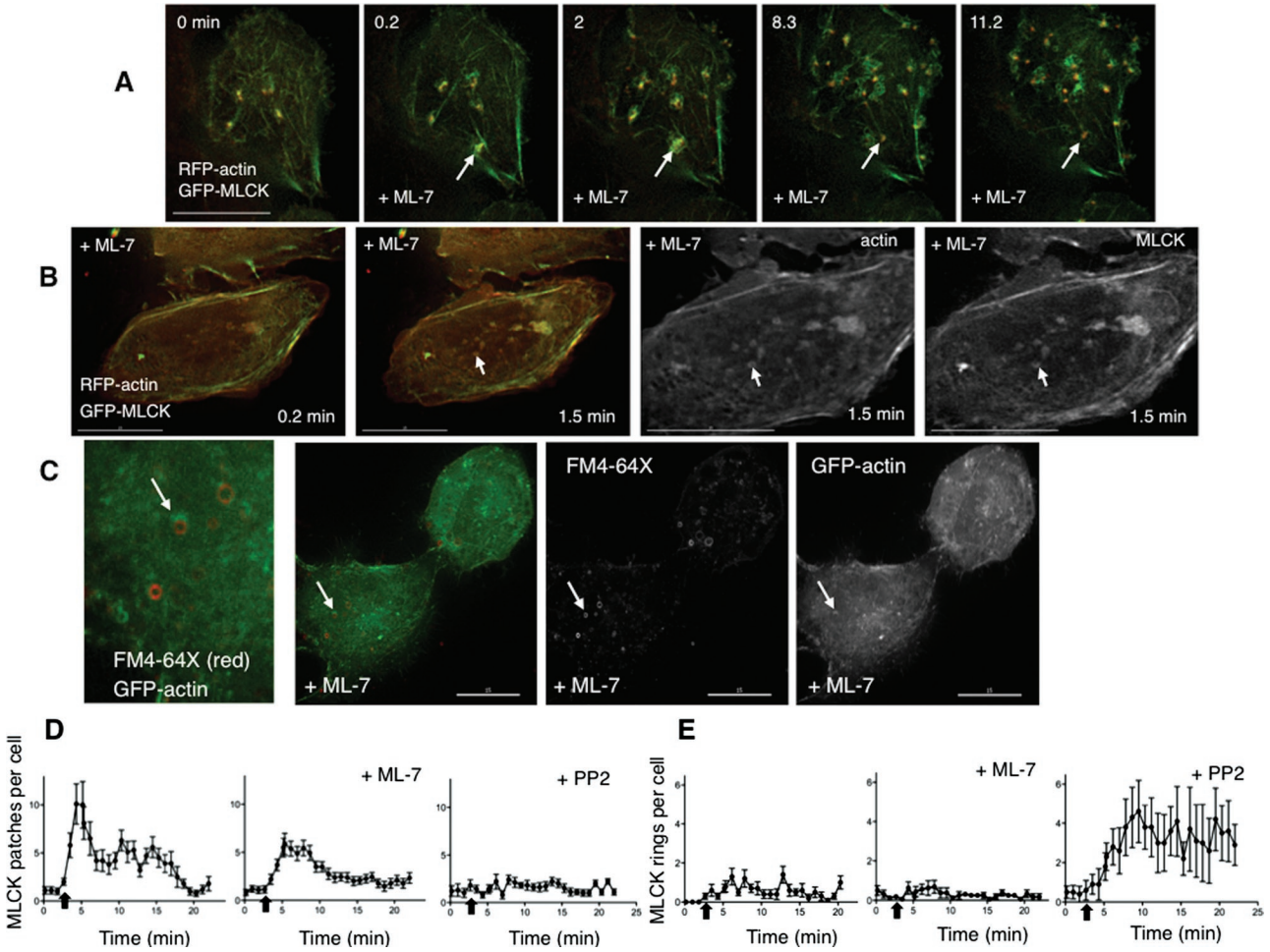

FIGURE 6: Inhibition of MLCK and of Src have distinct influences on patch and ring dynamics. (A) Stills from live imaging of the base of cells that were transfected with GFP-MLCK (green) and RFP-actin (red) and treated with the MLCK inhibitor ML-7 (10 μM) during hypotonic exposure (time in min). The arrow marks a transient MLCK patch for which the actin recruitment, accumulation, and departure parallel that of MLCK. The arrow in (B) marks an MLCK ring that also contains actin. Shown in the right two panels are the single channel signals for actin and MLCK at higher magnification of the 1.5-min time point. (C) Cells transfected with GFP-actin (green) were treated with exogenous FM4-64X (red) during hypotonic exposure in the presence of ML-7 (10 μM) and then fixed. Rings of actin and rings of FM4-64X membrane dye are seen alone and associated at the base of the cell (a magnified view is shown in the leftmost panel). An arrow marks an FM4-64X membrane ring on which actin partially surrounds the membrane ring. Shown in the right two panels are the single channel signals for FM4-64X and GFP-actin. Scale bars are 15 μm. (D) Graphs of the number of GFP-MLCK patches per cell, comparing hypotonic exposure in the presence and absence ML-7 (10 μM) or PP2 (10 μM) as a function of time. (E) Graphs of the number of GFP-MLCK rings per cell comparing hypotonic exposure in the presence and absence of ML-7 (10 μM) or PP2 (10 μM) as a function of time. Data in the leftmost graphs (absence of inhibitor) in panels D and E correspond to data presented in Figure 2C. All complete scale bars are 15 μm.

MLCK and actin at membrane rings raises the possibility that kinase activity of MLCK couples actin and MLCK function with membrane retrieval at these sites.

In contrast to ML-7, PP2 led to a significant increase in MLCK rings (maximum number of rings per cell at peak time: 2.3 ± 0.4 vs. 6.1 ± 1.6 with PP2, $p = 0.0334$). These findings support the concept that Src activity is responsible for the formation of volume-sensitive patches and that MLCK activity regulates patch turnover. Moreover the finding that Src inhibition led to ring accumulation suggests that ring maturation may require a Src-sensitive step to facilitate membrane internalization.

MLCK rings may represent MLCK-coated vesicle precursors

Some forms of endocytosis are regulated by lipid raft formation (Parton and Richards, 2003), which we have found to be important in cell volume control (Barfod *et al.*, 2007). In particular, Src activation has been suggested to control endocytosis mediated by GM1 ganglioside–containing lipid rafts (Shajahan *et al.*, 2004). To determine whether the sites of volume-sensitive membrane turnover we have observed were also enriched in such lipid raft domains, we exposed cells expressing GFP-MLCK to fluorescently labeled GM1 ganglioside marker cholera toxin B (CTXB) in addition to FM4-64X. When these cells were swollen in the presence of PP2 before fixation, distinct rings of MLCK and FM4-64X appeared within 1 min (Figure 7A), but no rings of CTXB were seen, although this marker was clearly internalized to separate compartments. However, the CTXB and FM4-64X signals did colocalize in intracellular vesicles at longer time points (10–15 min) after swelling (unpublished data), suggesting that the initial uptake mechanisms were distinct but that membrane mixing could occur subsequently in endosomes.

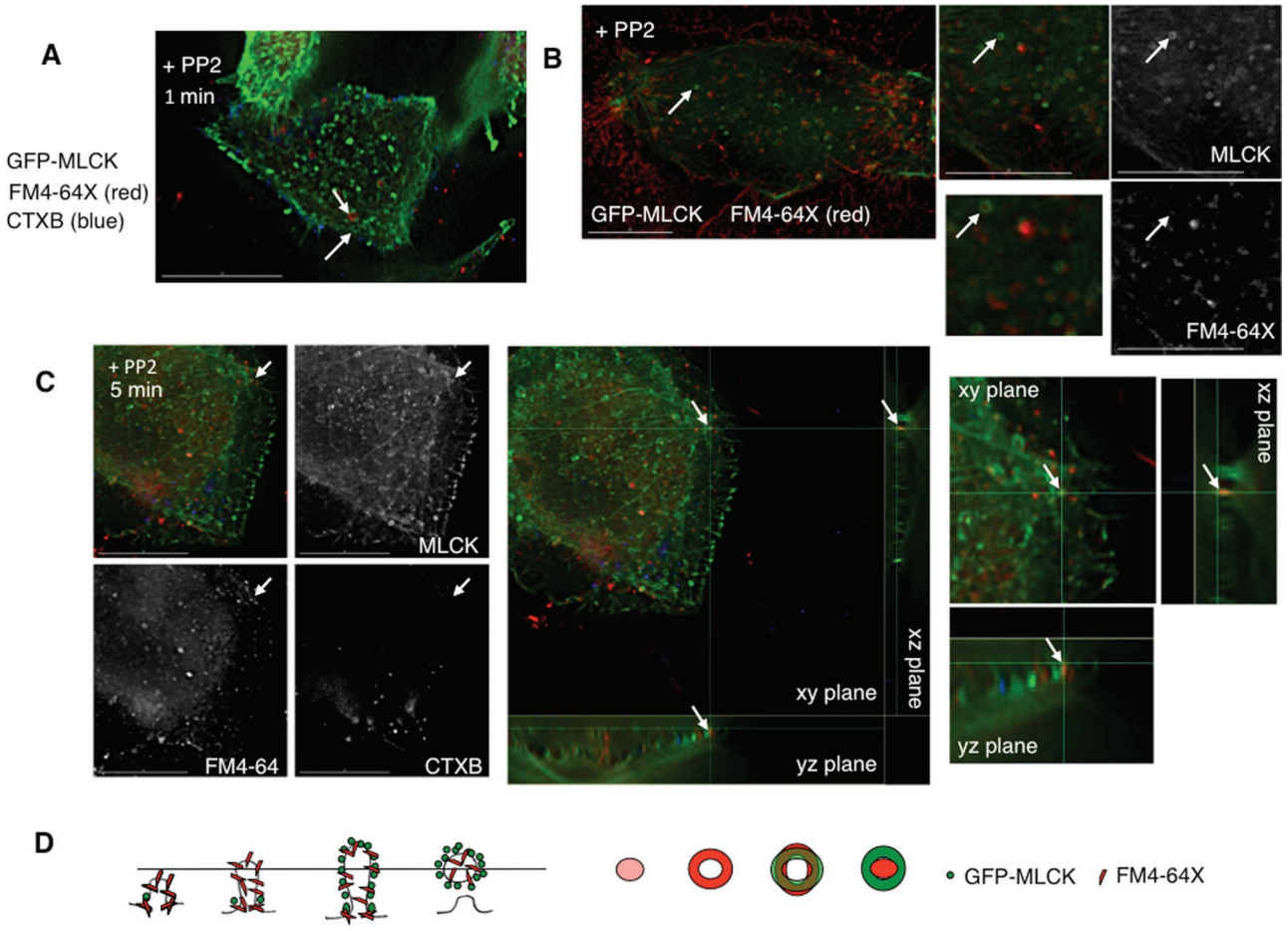

FIGURE 7: Src inhibition leads to the accumulation of internalized membrane marker within MLCK rings. MLCK rings may represent MLCK-coated vesicular intermediates. (A) Cells transfected with GFP-MLCK (green) were treated with exogenous FM4-64X (red) and fluorescently labeled CTXB (blue) during hypotonic exposure in the presence of PP2 (10 μM) for 1 min before fixation. Arrows mark distinct MLCK and FM4-64X membrane dye rings. (B) Stills from live imaging of cells transfected with GFP-MLCK (green) taken at the base and treated with PP2 (10 μM) during hypotonic treatment in the presence of exogenous FM4-64X. An arrow marks an MLCK ring that appears to encircle internalized membrane marker. (C) Cells transfected with GFP-MLCK (green) were treated with exogenous FM4-64X (red) and fluorescently labeled CTXB (blue) during hypotonic exposure in the presence of PP2 (10 μM) for 5 min before fixation. An arrow marks an MLCK ring that appears to encircle a lumen of FM4-64X–bound membrane dye. Single channel signals for MLCK, FM4-64X, and CTXB (left) show that FM4-64X signal is present in the ring, whereas CTXB signal is not. A three-dimensional reconstruction of the cell (right) with magnified panels adjacent shows that the MLCK ring surrounds FM4-64X dye. (D) Model for the visualization of rings. Side views of potential involuting membrane structures labeled with FM4-64X dye and recruited MLCK are marked with a plane of focus. The corresponding predicted two-dimensional patterns of FM4-64X and MLCK signal, as seen from above, are adjacent. Scale bars are 15 μm.

To further evaluate the structural relationship between MLCK and internalized membrane in rings under conditions of Src inhibition, we performed live imaging of GFP-MLCK–expressing cells undergoing hypotonic exposure in the presence of PP2 and FM4-64X. We found that under these conditions, MLCK could form rings that encircled a lumen that was homogeneously labeled by FM4-64X (Figure 7B). To gain additional insight into ring topology, we subjected GFP-MLCK–expressing cells to hypotonic exposure in the presence of PP2, with FM4-64X and CTXB to label sites of membrane and GM1 ganglioside uptake, respectively. We found localization of FM4-64X but not CTXB in MLCK-encircled structures (Figure 7C, left panel). Three-dimensional reconstruction of the image sections suggested that this structure represented a tethered plasma membrane vesicle encircled with MLCK (Figure 7C, middle panel and magnified insert). This concept is illustrated in the diagram in Figure 7D, which shows the potential relationship between MLCK ring/FM4-64X ring structures and MLCK ring/FM4-64X lumen-filled structures as a *z* line through a cross-sectional view and the corresponding *xy* views from above.

Cells expressing GFP-MLCK or GFP-dynamin form actin comets on cell swelling

During live imaging studies, we were intrigued to see MLCK-positive structures that appeared as comet tails, which increased in number upon hypotonic exposure in some GFP-MLCK–expressing cells (Figure 8A, Supplemental Video 19). These comets appeared most concentrated within 2 μm of the base of the cell, although they could be seen as high as 3 μm above the cell base. To investigate whether kinase function was necessary for comet formation, we transfected cells with mutant, kinase-inactive GFP-MLCK. Under

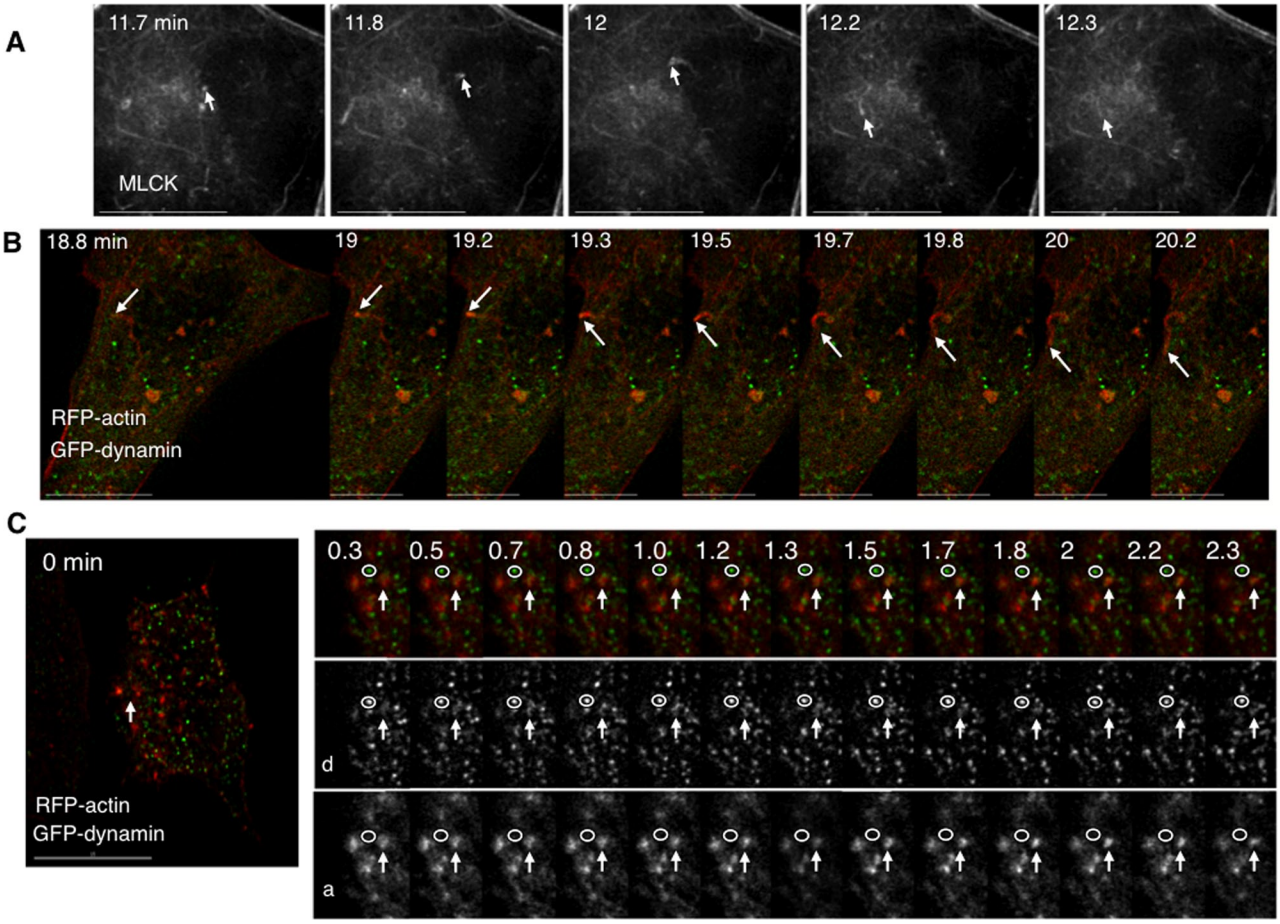

FIGURE 8: Cell swelling elicits formation of MLCK and actin comets. (A) Sequential stills from the base of a swollen cell expressing GFP-MLCK. An arrow points to a comet that arises and disappears. (B) Sequential stills from a cell expressing GFP-dynamin (green) and RFP-actin (red) during hypotonic exposure. An arrow marks an actin comet tail formed in response to cell swelling. (C) Sequential stills from a cell expressing GFP-dynamin (green) and RFP-actin (red) before and after hypotonic exposure. An arrow marks the position of an actin patch structure, the signal of which intensifies with cell swelling. A magnified view of that part of the cell includes the actin patch (arrow) and a punctum of dynamin that does not change on swelling or measurably localize with actin (circle). Single channel series depicting dynamin (d, middle) and actin (a, bottom) are below. Time (in min) indicates duration of hypotonic exposure. Scale bar is 15 μm except in B, where only the scale bar in the first panel is 15 μm.

these conditions, comets (as well as rings) were still observed upon hypotonic exposure (see Supplemental Videos 20 and 21), suggesting that kinase activity of MLCK is not required for their formation. In cells that were transfected only with GFP-MLCK, MLCK comets demonstrated a wide range of responses to cell swelling; these varied from no increase in the rate of comet formation to a 13-fold increase in the number of comets observed in a given cell (an absolute increase of 0–13.1 comets/min on cell swelling). Overall, the mean number of comets observed in each cell changed from 0.15 ± 0.07 per min under isotonic conditions to 2.18 ± 1.14 per min following hypotonic exposure, but this apparent increase was not statistically significant ($p = 0.1018$ by paired *t* test), potentially influenced by the wide range of responses observed. Given that actin comet tails are thought to be part of the final step mediating vesicle transport into the cytoplasm (Kaksonen *et al.*, 2005), we sought the involvement of other proteins known to be associated with actin comet formation.

Dynamin, a Src substrate and cortactin-binding protein (McNiven *et al.*, 2000) with an established role in endocytosis (Merrifield *et al.*, 2002; Pelkmans *et al.*, 2002; Cao *et al.*, 2010), has been shown to promote the appearance of actin-propelled vesicles (comet tails), particularly in the presence of costimulatory conditions (Lee and De Camilli, 2002; Orth *et al.*, 2002). Such studies have supported the concept that dynamin works in concert with actin polymerization to drive endocytosis by pinching off invaginating endosomal structures (Liu *et al.*, 2010). If actin polymerization played an analogous role in volume-sensitive membrane retrieval, it might be predicted that overexpression of dynamin would evoke actin comet tail formation upon cell swelling. To test this, we performed live imaging of cells transfected with GFP-dynamin and RFP-actin. Following hypotonic exposure, actin comet tails appeared (Figure 8B, Supplemental Video 22).

Dynamin associates with MLCK upon cell swelling and regulates volume recovery

Because dynamin responded to cell swelling by generating actin comet tails, we were interested whether it might play a functional role in volume recovery. To determine this, we compared the cell volume responses to hypotonic exposure in the presence versus absence of the dynamin inhibitor dynasore (Macia *et al.*, 2006). We found that dynasore indeed inhibited cell volume recovery (Figure 9C).

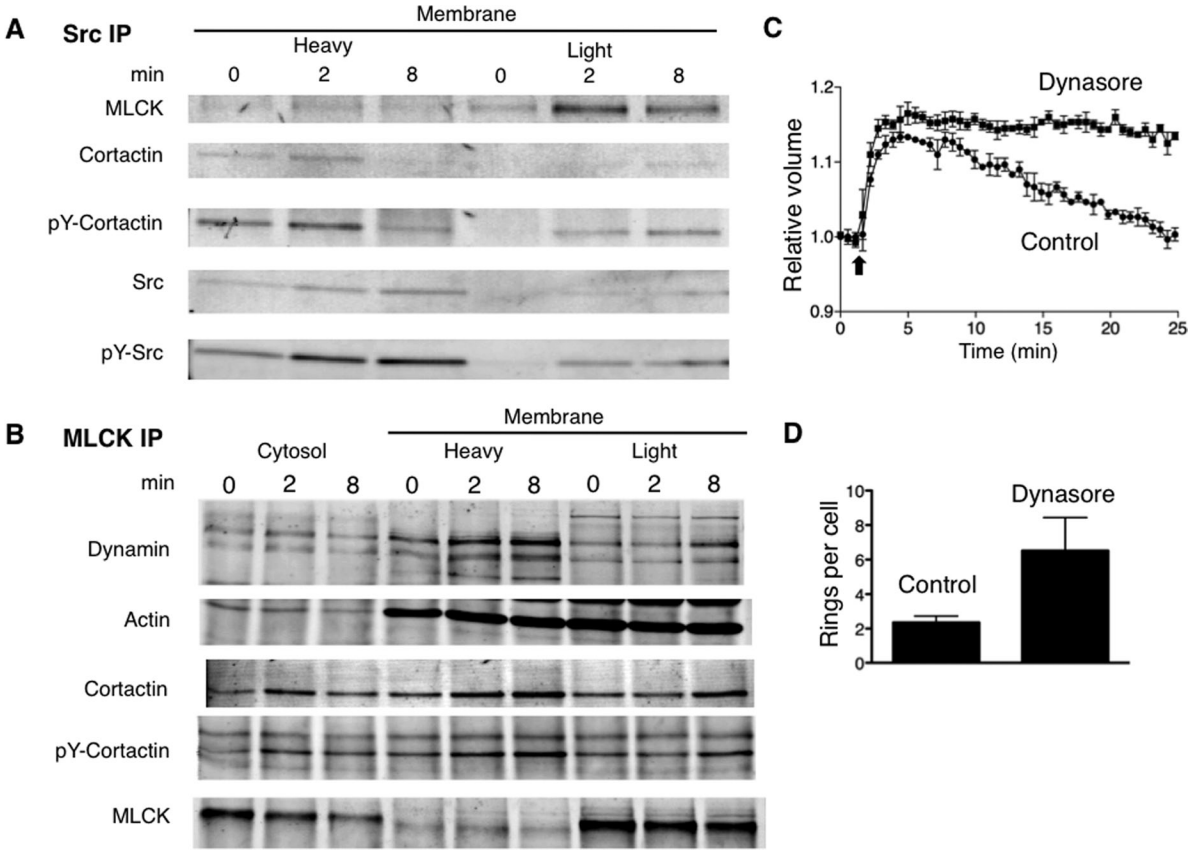

FIGURE 9: Dynamin is associated with MLCK in response to cell swelling and contributes to ring turnover and volume recovery. Lysates were extracted from cells under isotonic conditions (time = 0) and at different times (in min) after hypotonic exposure and then fractionated as described in *Materials and Methods*; heavy membrane fractions include plasma membrane, and light membrane fractions include small vesicles. Representative immunoblots of Src and MLCK immunoprecipitates of these fractions are shown in (A) and (B), respectively. (C) Effect of the dynamin inhibitor dynasore (80 μM) on cell volume recovery following hypotonic exposure (initiated at the time indicated by the arrow). (D) Effect of dynamin on MLCK ring abundance. GFP-MLCK–expressing cells were fixed after hypotonic exposure in the absence (control) or presence of dynasore (80 μM), and ring structures at the base were counted.

We next examined whether dynamin was associated with volume-sensitive MLCK/actin/cortactin patches. In live imaging studies of cells expressing RFP-actin and GFP-dynamin, we found that upon hypotonic exposure, GFP-dynamin was recruited to RFP-actin patches at the base of the cell (Figure 8C, Supplemental Figure S14, Supplemental Video 23). In parallel immunoprecipitation studies, we found that dynamin, like cortactin, associated with MLCK in membrane fractions in a time-dependent manner upon hypotonic exposure (Figure 9B). These findings are consistent with the concept that dynamin is recruited to a Src/MLCK/cortactin regulatory complex to facilitate a form of compensatory membrane retrieval under osmotic stress. If so, Src inhibition of dynamin activity would lead to suppression of endocytic vesicle scission and accumulation of presumptive MLCK-coated vesicles (i.e., rings), as we have observed. In support of this concept, we found that dynasore, like PP2, led to an accumulation of MLCK rings upon hypotonic exposure (Figure 9D, Supplemental Figure S13).

Swelling-induced MLCK rings at the base of the cell appear to arise from MLCK comets

We sought to examine how MLCK rings formed in response to cell swelling. Clues emerged from observations of MLCK comets that appeared to rocket in increasingly tighter spirals (Figure 10A, Supplemental Video 24). Occasionally, these were seen at the base of the cell to trace a path that appeared to form an MLCK ring that could persist. If a swelling-induced Src/MLCK/cortactin protein complex was responsible for actin polymerization on internalizing membranes, we predicted that we would detect MLCK moving around a ring of a marker of a presumably inwardly curving membrane. Our findings supported this. Live imaging of cells expressing GFP-MLCK swollen in the presence of FM4-64X indeed showed MLCK signal moving around an FM4-64X ring before an MLCK ring appeared (Figure 10B). Moreover, because we found that the kinase function of MLCK is not required for the generation of MLCK comets, it is likely that in this function of the complex, MLCK acts as a scaffolding protein that modulates the actin polymerization function of cortactin, analogous to models of dynamin-induced actin comet formation (Lee and De Camilli, 2002; Orth *et al.*, 2002).

The observation that MLCK inhibition slowed, but did not prevent, cell volume recovery after swelling (Figure 1G) suggests that ML-7 may not act with complete efficiency or that there may be some compensation for loss of MLCK. Indeed, during live imaging in the presence of ML-7, we occasionally observed at the base of the cell a ring of MLCK that collapsed to a point and disappeared over the course of minutes (Figure 10C, Supplemental Video 25). Similar morphologies were observed in cells that expressed

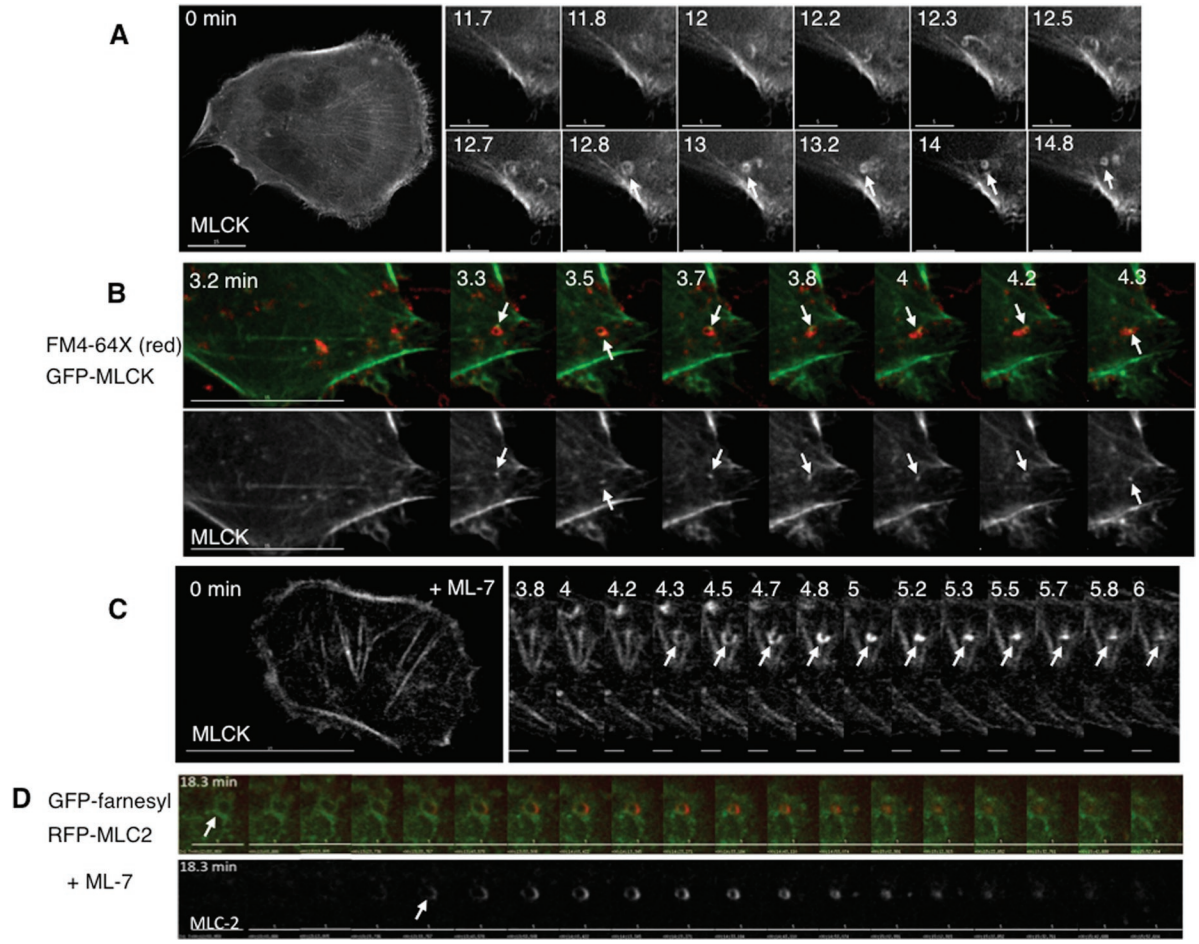

FIGURE 10: Dynamic behavior of MLCK and myosin II in swelling-induced rings. (A) Stills from a cell expressing GFP-MLCK, imaged before and after hypotonic exposure. The left panel shows the whole cell at 0 min (scale bar, 15 μm); the right panel shows a magnified region of the base at different times (in min) after hypotonic exposure (scale bar, 5 μm). An MLCK comet tail appears to form a ring (marked by an arrow), which persists for 2 min. (B) The top panel shows stills from a cell expressing GFP-MLCK (green) undergoing hypotonic exposure in the presence of FM4-64X (red). The bottom panel shows MLCK signal alone. An arrow marks a focus of MLCK signal that moves around an FM4-64X ring within 1 μm above the base of the cell. Scale bar is 15 μm. (C) In the presence of ML-7, MLCK rings can be seen to constrict slowly. The left panel shows the base of a GFP-MLCK–expressing cell just prior hypotonic treatment, and the kymograph in the right panel represents an enlarged region of the cell base with sequential images acquired at the indicated times (in min) after hypotonic exposure in the presence of ML-7 (10 μM). The arrow highlights the appearance and constriction of an MLCK ring in that cell. (D) Kymographs derived from sequential images (acquired every 10 s) of the base a cell expressing RFP-MLC2 (red) and GFP-farnesyl (green), exposed to hypotonic medium in the presence of ML-7 (10 μM). The arrow in the top panel highlights the formation of an MLC2/farnesyl ring that slowly constricts. The lower panel shows the MLC2 signal alone. Scale bar is 5 μm.

RFP-MLC2 (Figure 10D, Supplemental Video 26). This is striking because myosin II activation has been shown to stimulate macropinocytosis (Kolpak *et al.*, 2009), the endocytosis mode that most closely shares the properties of the MLCK rings. Moreover, the constriction patterns of the MLCK and MLC2 structures are reminiscent (although larger and with slower kinetics) of endocytic vesicle internalization as visualized by total internal reflectance microscopy (Merrifield *et al.*, 2002; Jaiswal and Simon, 2007). This raises the possibility that MLCK and myosin II provide constriction forces necessary for volume-sensitive membrane retrieval.

DISCUSSION

Osmotic stress causes dramatic changes in membrane tension and provokes bleb formation upon cell swelling. In common with other modes of membrane blebbing, we have found that myosin II localizes to blebs before their retraction. In our case, the actomyosin forces that power bleb retraction appear to be regulated by Src-activated MLCK and not ROCK. ROCK has been implicated in bleb retraction in processes that do not involve cell volume changes (Charras *et al.*, 2006; Fackler and Grosse, 2008), and it opposes MLCK-dependent tension in selected forms of cell motility (Totsukawa *et al.*, 2004). During cell swelling under conditions in which MLCK is inhibited, the formation of blebs in one region of the plasma membrane is accompanied by collapse of a bleb in another region (Figure 11A). By contrast, with ROCK and with myosin II ATPase inhibition, blebs do not form upon hypotonic exposure. We propose that during osmotic cell swelling, Src-activated MLCK acts to stabilize and promote repair of the actomyosin cortex and its connections with the plasma membrane. In support of this are the following: 1) our previous findings that Src is recruited to blebs

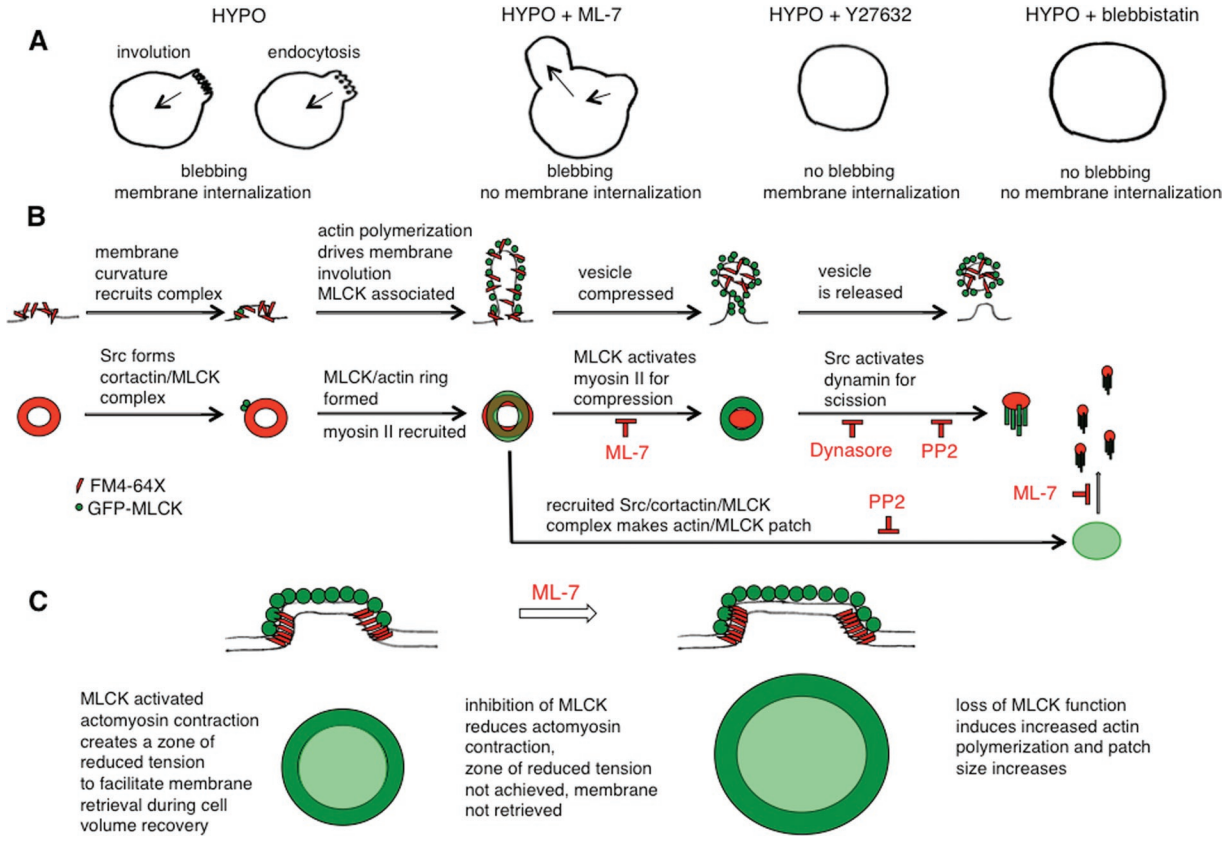

FIGURE 11: Models of MLCK and Src in control of membrane dynamics during osmotic stress. (A) In response to hypotonic swelling, a bleb membrane may be retracted with retrieval of added surface area by actomyosin-mediated involution or endocytosis. When MLCK is inhibited with ML-7, a bleb on a swollen cell can appear to collapse, but this occurs concomitantly with formation of another bleb and the total membrane area is not decreased. The inward membrane movement under these conditions is likely due to ROCK-mediated myosin II–dependent tension because inhibition of ROCK (with Y27632) and of myosin II (with blebbistatin) leads to cell swelling without bleb formation. Under hypotonic conditions when MLCK tension is reduced, the imbalance of unopposed ROCK tension pulls against cortical actin/membrane linkages to lead to bleb formation. (B) MLCK and Src could regulate volume-sensitive membrane retrieval at several levels, in analogy to the roles ascribed to actin and myosins in endocytic vesicle formation and internalization (Liu *et al.*, 2010). The first row of schematics indicates a potential set of intermediate stages of membrane retrieval, and the second row the correlated structures from our imaging data. Sites of specialized membrane curvature, which form in response to swelling, may recruit a Src/MLCK/cortactin complex that could promote cortactin-regulated actin polymerization to involute the membrane and stabilize it with an actin coat. Concomitant MLCK and myosin II recruitment would allow MLCK-activated myosin II to create zones of reduced membrane tension to allow endocytic machinery to act to facilitate cell volume recovery. In the macroscopic mode of membrane retrieval (rings), MLCK-activated myosin II could then drive actin coat compression (Yu and Bement, 2007). MLCK-activated myosin II may potentially also facilitate vesicle neck constriction (Bhat and Thorn, 2009) and act together with Src-activated dynamin, which is thought to be necessary but not sufficient for fission (Liu *et al.*, 2010). Inhibition of MLCK might be expected to slow the coat compression step of the macroscale endocytic (ring) mode and may influence a shift to the microscale (patch). Src function is required for the activation of dynamin, and thus inhibition of Src and of dynamin would be expected to lead to accumulation of prescission intermediates. (C) In contrast to rings, patches require the kinase function of Src for their formation. Once formed, patches require MLCK kinase activity to maintain their shape and size. We propose that the concomitant recruitment of actin and MLCK to patches represents the formation of an actomyosin network that stabilizes the patch periphery against the increased membrane tension of a swollen cell. In the absence of MLCK kinase function with sustained elevated membrane tension, patches enlarge. Thus Src-activated MLCK structures may provide fine-tuning of membrane tension to permit membrane retrieval in the face of hydrostatic pressure.

(Barfod *et al.*, 2005), where MLCK and its substrate myosin II are also recruited (this study), and 2) our findings with Src and MLCK inhibition, which suggest that Src-activated MLCK then phosphorylates myosin II and facilitates bleb retraction. When MLCK function is reduced, unopposed ROCK-mediated tension pulls the weakened actin cortex inward against the swelling-induced hydrostatic pressure, leading to local disruption of the cortical connections with the plasma membrane and consequent bleb formation. Thus, like nonosmotic blebbing, Src regulates membrane cortical actin connectivity and tension during osmotic stress, but, in contrast, it activates MLCK and not ROCK to achieve this end.

The increase in membrane tension elicited by hypotonic challenge suppresses endocytosis (Dai *et al.*, 1997), yet swollen cells must retrieve the membrane in order to achieve volume recovery

under these conditions. Src is well suited to control this process because its kinase activity is known to regulate membrane tension in other dynamic processes such as lamellipodial (Raucher and Sheetz, 2000) and axonal extension (Suter and Forscher, 2001), both of which depend on the modulation of myosin II activity. As a volume-sensitive myosin II regulator, MLCK is positioned to respond to localized swelling-induced increases in cell calcium (Moore *et al.*, 2002) because MLCK is activated by calmodulin, which is known to regulate different endocytic modes during changes in membrane tension (Wu *et al.*, 2009). Thus Src activation of MLCK can integrate spatial, signaling, and calcium cues for precise positioning of membrane retrieval. We propose that Src activation on cell swelling leads to the recruitment and activation of MLCK at the base of the cell to create zones of reduced membrane tension that facilitate membrane retrieval by two different mechanisms, one macroscopic (rings) and one microscopic (patches).

Our findings suggest that rings and patches are sites of membrane internalization, as they dynamically label with membrane-bound probes in response to cell swelling. Inhibition of Src kinase and dynamin GTPase functions reduces cell volume recovery and leads to an increase in MLCK-coated rings and their association with membrane rings. Inhibition of MLCK kinase function also reduces cell volume recovery and leads to an increase in MLCK-associated patches. We therefore propose that membrane retrieval through patches and rings involves the formation of a volume-sensitive Src/MLCK/cortactin complex that also recruits dynamin. This is supported by our identification of such a complex by immunoprecipitation and imaging studies as well as by our observations regarding the spatial and temporal coincidence of Src activation and influence of protein kinase inhibition on ring and patch dynamics. With Src inhibition, there was an apparent reduction in the formation and/or stability of MLCK patches upon cell swelling, whereas with MLCK inhibition, MLCK patch size and lifetime increased. This implies a role for Src in patch formation and for MLCK in patch turnover. The accumulation of apparent MLCK-encircled tethered vesicles with Src and dynamin inhibition suggests that Src kinase activity is required as well as dynamin for a scission step, similar to those described for endocytosis. Thus Src, dynamin, cortactin, and MLCK are likely to have overlapping but distinct regulatory roles in volume-sensitive compensatory membrane internalization. Src could influence MLCK/actin patch and ring formation and stability by coordinating the formation of distinct MLCK or dynamin-containing protein complexes, analogous to its role in stimulating the formation of a Src/cortactin/dynamin complex for clathrin-mediated endocytosis (Cao *et al.*, 2010). A conceptual model for this is presented in Figure 11, B and C.

How might MLCK function in actin patches? Kinase inhibition of MLCK increases patch diameter and lifetime, consistent with a defect in patch turnover and consistent with the possibility that myosin II is involved in patch dynamics as well. Intriguingly, myosin II, within a bridging network of actomyosin, can stabilize the plasma membrane at the base of the cell across nonadherent regions under force from adjacent adherent regions (Rossier *et al.*, 2010). It is thus tempting to speculate that under osmotic stress, such an actomyosin network could stabilize the edges of a patch against the elevated tension of the rest of the plasma membrane to create a lower tension area for membrane retrieval.

Given that osmotically induced swelling involves contributions from the addition of membrane, a unifying hypothesis would be that Src-activated MLCK modulates not only membrane dynamics during bleb retraction but also membrane retrieval at the base of the cell as a compensatory response. In light of our observations and the hypotheses proposed above, we therefore propose that volume-sensitive compensatory membrane retrieval and its regulation by Src and MLCK represent a new example of a general mechanism for coordinating protrusive or invaginating membrane dynamics in response to changes in membrane tension.

MATERIALS AND METHODS

Reagents and antibodies

The membrane dye FM4-64X, Alexa 488– and Alexa 568–conjugated anti–rabbit and anti–mouse antibodies, Alexa 647–conjugated CTXB, Alex 647 fluorescent dextran (10 kDa), and the donkey anti–rabbit and anti–mouse Alexa 680 antibodies were purchased from Invitrogen, Carlsbad, CA. Cy3- and Cy5-conjugated anti–mouse and anti–rabbit antibodies were purchased from Jackson ImmunoResearch Laboratories (West Grove, PA). The IRDye 800–conjugated donkey anti–goat and goat anti–mouse antibodies were from Rockland Immunochemicals (Gilbertsville, PA). Activated pY-specific Src family (Y416) rabbit polyclonal antibodies; the mouse monoclonal antibody (mAb) against the phosphoserine, activated form of the regulatory light chain of myosin II (Ser19); and the rabbit polyclonal antibodies directed against the diphosphorylated, activated form of the regulatory light chain of myosin II (Thr18, Ser19) were obtained from Cell Signaling, Danvers, MA. The mouse monoclonal glyceraldehyde-3-phosphate dehydrogenase antibody (6C5), monoclonal pp60Src antibody (clone GD11) and the GD11-agarose conjugate, the pY-specific Src family (Y416) mouse mAb (9A6) used for immunostaining, mouse monoclonal dynamin antibody (Hudy1), p80/p85 cortactin mouse mAb (clone 4F11), and the pY-specific cortactin (Y486) rabbit polyclonal antibodies were purchased from Millipore, Billerica, MA. Goat polyclonal anti-MLCK antibody (P19 MYLK), Protein G PLUS-Agarose, and the mouse monoclonal against the regulatory light chain of myosin II (MY21) were from Santa Cruz Biotechnology (Santa Cruz, CA). ML-7, Y27632, PP2, dynasore, the phosphatase inhibitor mixture Set II, bpV(phen), and NP-40 were obtained from EMD, Calbiochem, San Diego, CA. The protease inhibitor (HALT) was obtained from Pierce, Rockford, IL. Na_4BAPTA was from (Fluka, Sigma-Aldrich, St. Louis, MO). Aquablock was purchased from EastCoast Bio (North Berwick, ME). All other reagents were from Sigma unless specifically noted.

Cell culture, fusion construction, and transfections

HTC rat hepatoma cells were maintained in culture and transfected using Amaxa nucleofector technology (program T20, Lonza, Basel, Switzerland) as previously described (Barfod *et al.*, 2007). A fusion of the H-ras farnesyl group with GFP was a kind gift from Jim Koh (University of Vermont, Burlington, VT). This fusion contains a small domain of H-ras, which undergoes farnesylation and palmitoylation and thus targets the protein to membranes to allow long-term fluorescent labeling (Prior *et al.*, 2001). The GFP was replaced with RFP to create an RFP-farnesyl fusion by standard subcloning using mCherry-N1 plasmid (Invitrogen, Clontech). The GFP-actin fusion was kindly provided by John Burke (University of Vermont). The RFP-actin was a kind gift from Roger Tsien (University of California San Diego). A DSRed2-fusion of the regulatory light chain of myosin II was kindly provided by Daniel Ortiz (Tufts University, Boston, MA). The yellow fluorescent protein (YFP) tandem Src dSH2 and GFP-Arp3 fusions were a kind gift from Alan Howe (University of Vermont). GFP-cortactin and GFP-dynamin fusions were kindly provided by Anthony Morielli (University of Vermont). The GFP was replaced with RFP to create an RFP-cortactin fusion by standard subcloning using the mCherry-N1 plasmid (Invitrogen, Clontech). The GFP fusions of the long form of MLCK and of its kinase-inactive (E1626K) mutant were

generously provided by Anne Bresnick (Albert Einstein College of Medicine, Bronx, NY).

Live imaging and cell volume analysis

Transfected cells were plated onto glass coverslips and imaged from 18 to 48 h after plating. Imaging proceeded essentially as described before (Barfod *et al.*, 2005), except that the stage of the DeltaVision Restoration Olympus IX70 microscope was heated to 37°C, and 60× oil (NA 1.4) or 100× oil lenses (NA 1.4) were used. For most time-lapse experiments, four 1-µm z sections were obtained every 10 s. First, cells were imaged for 5 min in isotonic extracellular solution (SES, ~300 mOsm) that contained 140 mM NaCl, 4 mM KCl, 1 mM $CaCl_2$, 2 mM $MgCl_2$, 1 mM KH_2PO_4, 10 mM glucose, and 10 mM HEPES (pH 7.4). They were then exposed to hypotonic extracellular solution (HYPO, ~240 mOsm, identical to SES except for a reduction of NaCl from 140 mM to 84 mM) and imaged for a further 20 min. When used, inhibitors were provided with the HYPO. Data collection, deconvolution, and imaging analysis were made with DeltaVision softWoRx version 3.71 (Applied Precision, Issaquah, WA). Linear adjustments to brightness and contrast were made. Cell volume measurements were made in suspended cells with a Multisizer 3 Coulter Counter as before (Barfod *et al.*, 2007), except that after cells were trypsinized they were rotated in complete media for 20 min at 37°C to restore the plasma membrane. Cells were spun and brought up in SES with and without inhibitors and gently mixed for an additional 15 min before beginning the Coulter measurements.

Immunoblot, immunoprecipitation, and immunofluorescence

The immunoprecipitation and immunofluorescence experiments were performed as described before (Barfod *et al.*, 2005). The immunoblots of whole cell lysates were done as described before (Moore *et al.*, 2002) except with an enhanced radio immunoprecipitation assay buffer: 50 mM Tris, pH 7.5, 150 mM NaCl, 1 mM EDTA, 1% NP40, 0.25% sodium deoxycholate, 1% SDS, and 10% glycerol, and added fresh the day of experiment: 1 mM dithiothreitol, 1 mM sodium vanadate, 1 mM NaF, phenylmethylsulfonyl fluoride, HALT protease inhibitor cocktail, phosphatase inhibitor cocktail 11, 0.01 mg/ml bpV(phen), 1 mM Na_4BAPTA, and 2 mM ATP. Crude membrane and cytosolic fractions were obtained as previously described (Barfod *et al.*, 2005) with the addition of 0.01 mg/ml bpV(phen), 1 mM Na_4BAPTA, and 2 mM ATP in the extraction buffer and the membrane pellet solubilization buffer. Briefly, the cells were homogenized in cold extraction buffer and centrifuged at low speed 10 min at 800 × *g* to remove debris, and then the supernatant was centrifuged at 50,000 × *g* for 30 min. The cytosolic supernatant was removed and recentrifuged at 100,000 × *g* for 60 min. The pellets were solubilized in membrane solubilization buffer. The 50,000 × *g* pellet was considered to contain the heavy membrane fraction (including plasma membrane), and the 100,000 × *g* pellet was considered to be the light membrane fraction that includes small vesicles. These fractions were either used directly in immunoblots or in immunoprecipitation experiments using goat polyclonal anti-MLCK antibody (P19 MYLK) and Protein G PLUS-Agarose or monoclonal pp60Src antibody (clone GD11) agarose conjugate. Gels were blotted on polyvinylidene difluoride membranes, blocked using a 1:1 mixture of AquaBlock and Tris-buffered saline, and labeled with appropriate primary antibodies and infrared secondary antibodies. Membranes were scanned using the LI-COR Odyssey Infrared Imager (Lincoln, NE). Bands were quantified using the Odyssey analysis software.

Image quantification

For the size and lifetime determinations of GFP-MLCK patches and rings, only those structures that appeared for more than one 10-s time point were used. Structures smaller than 0.3 µm in diameter were not included. In the experiments performed to determine the time dependence of YFP-tandem dSH2 flashes and GFP-MLCK patch and ring appearance, cells were cotransfected with RFP-MLC2 to act as a cytoplasmic marker. Structures near the periphery of cells were not counted to avoid contributions from lamellipodia, focal adhesions, and other extraneous peripheral membrane remodeling events. Because of their dynamic accumulation over time, for the quantification of MLCK rings associated with farnesyl or FM4-64X rings, MLCK signal associated with membrane rings in a curved shape was counted as positive (for example, the MLCK ring marked with an arrow in Figure 6C is a positive). Colocalization analysis of fixed cells was performed using the ROI colocalization option in the DeltaVision softWoRx program. Quantification of live imaging signals over time used a line segment drawn across the structure of interest within the softWoRx program. Pixel intensities along the line for the different wavelengths at each time point were exported into Excel (version 12.2.7) and graphed.

Statistics

Results are presented as means plus or minus standard error of the mean. Comparisons of means were made with the use of paired or unpaired Student's *t* test, as appropriate, and $p < 0.05$ was considered to be significant. Correlation coefficients were determined by nonparametric statistical analysis (Spearman), and significance was determined with two-tailed analysis at the 95% confidence level, using Prism version 5.0cx (GraphPad Software, La Jolla, CA).

ACKNOWLEDGMENTS

We thank Todd Clason (Neuroscience Imaging Core, University of Vermont) for helpful discussions in acquiring and interpreting live images. We also thank Jim Koh, John Burke, Roger Tsien, Daniel Ortiz, Anthony Morielli, Alan Howe, and Anne Bresnick for plasmids. We are grateful to Anthony Morielli, Matthew Lord, Todd Clason, and Michael Williams for helpful discussions and critical reading of the manuscript. This project was supported in part by National Institutes of Health (NIH) Grant DK-56644 (to SDL). The automated DNA sequencing was performed in the Vermont Cancer Center DNA Analysis Facility and was supported in part by Grant P30CA22435 from the National Cancer Institute, the NIH, and in part by the Vermont Cancer Center and the UVM College of Medicine. Use of the LI-COR Odyssey Infrared Imager and use of the DeltaVision restoration microscope were provided through the Cellular and Molecular Core and Neuroscience Imaging Core, respectively, supported by NIH Grant P20 RR-16435 from the Center of Biomedical Research Excellence program of the National Center for Research Resources.

REFERENCES

Ammer AG, Weed SA (2008). Cortactin branches out: roles in regulating protrusive actin dynamics. Cell Motil Cytoskeleton 65, 687–707.

Andzelm MM, Chen X, Krzewski K, Orange JS, Strominger JL (2007). Myosin IIA is required for cytolytic granule exocytosis in human NK cells. J Exp Med 204, 2285–2291.

Barfod ET, Moore AL, Melnick RF, Lidofsky SD (2005). Src regulates distinct pathways for cell volume control through Vav and phospholipase Cγ. J Biol Chem 280, 25548–25557.

Barfod ET, Moore AL, Roe MW, Lidofsky SD (2007). Ca^{2+}-activated IK1 channels associate with lipid rafts upon cell swelling and mediate volume recovery. J Biol Chem 282, 8984–8993.

Bement WM, Benink H, Mandato CA, Swelstad BB (2000). Evidence for direct membrane retrieval following cortical granule exocytosis in *Xenopus* oocytes and eggs. J Exp Zool 286, 767–775.
Bhat P, Thorn P (2009). Myosin 2 maintains an open exocytic fusion pore in secretory epithelial cells. Mol Biol Cell 20, 1795–1803.
Birukov KG, Csortos C, Marzilli L, Dudek S, Ma SF, Bresnick AR, Verin AD, Cotter RJ, Garcia JG (2001). Differential regulation of alternatively spliced endothelial cell myosin light chain kinase isoforms by p60(Src). J Biol Chem 276, 8567–8573.
Cao H, Chen J, Krueger EW, McNiven MA (2010). SRC-mediated phosphorylation of dynamin and cortactin regulates the "constitutive" endocytosis of transferrin. Mol Cell Biol 30, 781–792.
Cao H, Orth JD, Chen J, Weller SG, Heuser JE, McNiven MA (2003). Cortactin is a component of clathrin-coated pits and participates in receptor-mediated endocytosis. Mol Cell Biol 23, 2162–2170.
Charras GT (2008). A short history of blebbing. J Microsc 231, 466–478.
Charras GT, Coughlin M, Mitchison TJ, Mahadevan L (2008). Life and times of a cellular bleb. Biophys J 94, 1836–1853.
Charras GT, Hu CK, Coughlin M, Mitchison TJ (2006). Reassembly of contractile actin cortex in cell blebs. J Cell Biol 175, 477–490.
Cohen DM (2005). SRC family kinases in cell volume regulation. Am J Physiol Cell Physiol 288, C483–493.
Dai J, Ting-Beall HP, Sheetz MP (1997). The secretion-coupled endocytosis correlates with membrane tension changes in RBL 2H3 cells. J Gen Physiol 110, 1–10.
Dudek SM, Birukov KG, Zhan X, Garcia JG (2002). Novel interaction of cortactin with endothelial cell myosin light chain kinase. Biochem Biophys Res Commun 298, 511–519.
Engqvist-Goldstein AE, Zhang CX, Carreno S, Barroso C, Heuser JE, Drubin DG (2004). RNAi-mediated Hip1R silencing results in stable association between the endocytic machinery and the actin assembly machinery. Mol Biol Cell 15, 1666–1679.
Fackler OT, Grosse R (2008). Cell motility through plasma membrane blebbing. J Cell Biol 181, 879–884.
Feranchak AP, Lewis MA, Kresge C, Sathe M, Bugde A, Luby-Phelps K, Antich PP, Fitz JG (2010). Initiation of purinergic signaling by exocytosis of ATP-containing vesicles in liver epithelium. J Biol Chem 285, 8138–8147.
Garcia JG, Verin AD, Schaphorst K, Siddiqui R, Patterson CE, Csortos C, Natarajan V (1999). Regulation of endothelial cell myosin light chain kinase by Rho, cortactin, and p60(src). Am J Physiol 276, L989–998.
Gatof D, Kilic G, Fitz JG (2004). Vesicular exocytosis contributes to volume-sensitive ATP release in biliary cells. Am J Physiol Gastrointest Liver Physiol 286, G538–546.
Giannone G, Dubin-Thaler BJ, Dobereiner HG, Kieffer N, Bresnick AR, Sheetz MP (2004). Periodic lamellipodial contractions correlate with rearward actin waves. Cell 116, 431–443.
Haller T, Dietl P, Pfaller K, Frick M, Mair N, Paulmichl M, Hess MW, Furst J, Maly K (2001). Fusion pore expansion is a slow, discontinuous, and Ca^{2+}-dependent process regulating secretion from alveolar type II cells. J Cell Biol 155, 279–289.
Head JA, Jiang D, Li M, Zorn LJ, Schaefer EM, Parsons JT, Weed SA (2003). Cortactin tyrosine phosphorylation requires Rac1 activity and association with the cortical actin cytoskeleton. Mol Biol Cell 14, 3216–3229.
Hoffmann EK, Lambert IH, Pedersen SF (2009). Physiology of cell volume regulation in vertebrates. Physiol Rev 89, 193–277.
Jaiswal JK, Simon SM (2007). Imaging single events at the cell membrane. Nat Chem Biol 3, 92–98.
Jiang J, Kolpak AL, Bao ZZ (2010). Myosin IIB isoform plays an essential role in the formation of two distinct types of macropinosomes. Cytoskeleton (Hoboken) 67, 32–42.
Kaksonen M, Toret CP, Drubin DG (2005). A modular design for the clathrin- and actin-mediated endocytosis machinery. Cell 123, 305–320.
Kasahara K, Nakayama Y, Sato I, Ikeda K, Hoshino M, Endo T, Yamaguchi N (2007). Role of Src-family kinases in formation and trafficking of macropinosomes. J Cell Physiol 211, 220–232.
Kirchner J, Kam Z, Tzur G, Bershadsky AD, Geiger B (2003). Live-cell monitoring of tyrosine phosphorylation in focal adhesions following microtubule disruption. J Cell Sci 116, 975–986.
Kolpak AL, Jiang J, Guo D, Standley C, Bellve K, Fogarty K, Bao ZZ (2009). Negative guidance factor-induced macropinocytosis in the growth cone plays a critical role in repulsive axon turning. J Neurosci 29, 10488–10498.
Kumari S, Mg S, Mayor S (2010). Endocytosis unplugged: multiple ways to enter the cell. Cell Res 20, 256–275.
Lee E, De Camilli P (2002). Dynamin at actin tails. Proc Natl Acad Sci USA 99, 161–166.
Liu J, Sun Y, Oster GF, Drubin DG (2010). Mechanochemical crosstalk during endocytic vesicle formation. Curr Opin Cell Biol 22, 36–43.
Macia E, Ehrlich M, Massol R, Boucrot E, Brunner C, Kirchhausen T (2006). Dynasore, a cell-permeable inhibitor of dynamin. Dev Cell 10, 839–850.
Marchiando AM *et al.* (2010). Caveolin-1-dependent occludin endocytosis is required for TNF-induced tight junction regulation in vivo. J Cell Biol 189, 111–126.
McNiven MA, Cao H, Pitts KR, Yoon Y (2000). The dynamin family of mechanoenzymes: pinching in new places. Trends Biochem Sci 25, 115–120.
Merrifield CJ, Feldman ME, Wan L, Almers W (2002). Imaging actin and dynamin recruitment during invagination of single clathrin-coated pits. Nat Cell Biol 4, 691–698.
Merrifield CJ, Perrais D, Zenisek D (2005). Coupling between clathrin-coated-pit invagination, cortactin recruitment, and membrane scission observed in live cells. Cell 121, 593–606.
Moore AL, Roe MW, Melnick RF, Lidofsky SD (2002). Calcium mobilization evoked by hepatocellular swelling is linked to activation of phospholipase Cγ. J Biol Chem 277, 34030–34035.
Mulholland J, Preuss D, Moon A, Wong A, Drubin D, Botstein D (1994). Ultrastructure of the yeast actin cytoskeleton and its association with the plasma membrane. J Cell Biol 125, 381–391.
Musch MW, Koomoa DL, Goldstein L (2004). Hypotonicity-induced exocytosis of the skate anion exchanger skAE1: role of lipid raft regions. J Biol Chem 279, 39447–39453.
Nilius B, Prenen J, Walsh MP, Carton I, Bollen M, Droogmans G, Eggermont J (2000). Myosin light chain phosphorylation-dependent modulation of volume-regulated anion channels in macrovascular endothelium. FEBS Lett 466, 346–350.
Orth JD, Krueger EW, Cao H, McNiven MA (2002). The large GTPase dynamin regulates actin comet formation and movement in living cells. Proc Natl Acad Sci USA 99, 167–172.
Parton RG, Richards AA (2003). Lipid rafts and caveolae as portals for endocytosis: new insights and common mechanisms. Traffic 4, 724–738.
Pelkmans L, Puntener D, Helenius A (2002). Local actin polymerization and dynamin recruitment in SV40-induced internalization of caveolae. Science 296, 535–539.
Prior IA, Harding A, Yan J, Sluimer J, Parton RG, Hancock JF (2001). GTP-dependent segregation of H-ras from lipid rafts is required for biological activity. Nat Cell Biol 3, 368–375.
Raucher D, Sheetz MP (2000). Cell spreading and lamellipodial extension rate is regulated by membrane tension. J Cell Biol 148, 127–136.
Rey M, Valenzuela-Fernandez A, Urzainqui A, Yanez-Mo M, Perez-Martinez M, Penela P, Mayor F Jr, Sanchez-Madrid F (2007). Myosin IIA is involved in the endocytosis of CXCR4 induced by SDF-1alpha. J Cell Sci 120, 1126–1133.
Robles E, Woo S, Gomez TM (2005). Src-dependent tyrosine phosphorylation at the tips of growth cone filopodia promotes extension. J Neurosci 25, 7669–7681.
Rossier OM *et al.* (2010). Force generated by actomyosin contraction builds bridges between adhesive contacts. EMBO J 29, 1055–1068.
Saffarian S, Cocucci E, Kirchhausen T (2009). Distinct dynamics of endocytic clathrin-coated pits and coated plaques. PLoS Biol 7, e1000191.
Sauvonnet N, Dujeancourt A, Dautry-Varsat A (2005). Cortactin and dynamin are required for the clathrin-independent endocytosis of γc cytokine receptor. J Cell Biol 168, 155–163.
Schliess F, Reinehr R, Haussinger D (2007). Osmosensing and signaling in the regulation of mammalian cell function. FEBS J 274, 5799–5803.
Shajahan AN, Timblin BK, Sandoval R, Tiruppathi C, Malik AB, Minshall RD (2004). Role of Src-induced dynamin-2 phosphorylation in caveolae-mediated endocytosis in endothelial cells. J Biol Chem 279, 20392–20400.
Shen MR, Furla P, Chou CY, Ellory JC (2002). Myosin light chain kinase modulates hypotonicity-induced Ca^{2+} entry and Cl^- channel activity in human cervical cancer cells. Pflugers Arch 444, 276–285.
Sokac AM, Bement WM (2006). Kiss-and-coat and compartment mixing: coupling exocytosis to signal generation and local actin assembly. Mol Biol Cell 17, 1495–1502.
Sokac AM, Co C, Taunton J, Bement W (2003). Cdc42-dependent actin polymerization during compensatory endocytosis in *Xenopus* eggs. Nat Cell Biol 5, 727–732.
Straub SG, Daniel S, Sharp GW (2002). Hyposmotic shock stimulates insulin secretion by two distinct mechanisms. Studies with the βHC9 cell. Am J Physiol Endocrinol Metab 282, E1070–1076.

Suter DM, Forscher P (2001). Transmission of growth cone traction force through apCAM-cytoskeletal linkages is regulated by Src family tyrosine kinase activity. J Cell Biol 155, 427–438.
Sverdlov M, Shajahan AN, Minshall RD (2007). Tyrosine phosphorylation-dependence of caveolae-mediated endocytosis. J Cell Mol Med 11, 1239–1250.
Thorn P, Fogarty KE, Parker I (2004). Zymogen granule exocytosis is characterized by long fusion pore openings and preservation of vesicle lipid identity. Proc Natl Acad Sci USA 101, 6774–6779.
Togo T, Steinhardt RA (2004). Nonmuscle myosin IIA and IIB have distinct functions in the exocytosis-dependent process of cell membrane repair. Mol Biol Cell 15, 688–695.
Totsukawa G, Wu Y, Sasaki Y, Hartshorne DJ, Yamakita Y, Yamashiro S, Matsumura F (2004). Distinct roles of MLCK and ROCK in the regulation of membrane protrusions and focal adhesion dynamics during cell migration of fibroblasts. J Cell Biol 164, 427–439.
Tournaviti S, Hannemann S, Terjung S, Kitzing TM, Stegmayer C, Ritzerfeld J, Walther P, Grosse R, Nickel W, Fackler OT (2007). SH4-domain-induced plasma membrane dynamization promotes bleb-associated cell motility. J Cell Sci 120, 3820–3829.
Van Der Wijk T, Tomassen SF, Houtsmuller AB, de Jonge HR, Tilly BC (2003). Increased vesicle recycling in response to osmotic cell swelling. Cause and consequence of hypotonicity-provoked ATP release. J Biol Chem 278, 40020–40025.
Vicente-Manzanares M, Ma X, Adelstein RS, Horwitz AR (2009). Non-muscle myosin II takes centre stage in cell adhesion and migration. Nat Rev Mol Cell Biol 10, 778–790.
Wilkerson EH, DiBona DR, Schafer JA (1986). Analysis of structural changes during hypotonic swelling in Ehrlich ascites tumor cells. Am J Physiol 251, C104–C114.
Worrell RT, Butt AG, Cliff WH, Frizzell RA (1989). A volume-sensitive chloride conductance in human colonic cell line T84. Am J Physiol 256, C1111–C1119.
Wu XS, McNeil BD, Xu J, Fan J, Xue L, Melicoff E, Adachi R, Bai L, Wu LG (2009). Ca^{2+} and calmodulin initiate all forms of endocytosis during depolarization at a nerve terminal. Nat Neurosci 12, 1003–1010.
Yarar D, Waterman-Storer CM, Schmid SL (2005). A dynamic actin cytoskeleton functions at multiple stages of clathrin-mediated endocytosis. Mol Biol Cell 16, 964–975.
Yu HY, Bement WM (2007). Multiple myosins are required to coordinate actin assembly with coat compression during compensatory endocytosis. Mol Biol Cell 18, 4096–4105.